intrinsic reactive oxygen species (ROS) production [14,18,19]. Since accumulation of intrinsic ROS levels could be a major reason for replicative senescence [20], enhancing glycolysis in cultured cells might improve the quality of the cells by suppressing premature senescence. One candidate method for induction of glycolysis is application of low-oxygen conditions to activate the transcription factor, hypoxia-inducible factor (HIF). HIF-1 is known to increase the expression of most glycolytic enzymes and the glucose transporters GLUT1 and GLUT3 [20]. Thus, several studies have reported that hypoxia is beneficial for the maintenance of hESCs in a pluripotent state [21,22]. Moreover, low oxygen tension has been reported to enhance the generation of iPSCs both from mouse and human primary fibroblasts [23].

Recently, hypoxic culture conditions have also been reported to confer a growth advantage, prevent premature senescence, and maintain undifferentiated states in somatic stem cells; for example, hematopoietic stem cells (HSCs) [24], neural stem cells [25], and bone marrow-derived MSCs [26]. These stem cells reside in their local microenvironments called the "stem cell niche," where the oxygen tension is relatively low (in the range of 1%–9%). Thus, hypoxic culture may be beneficial to these stem cells with regard to in vitro proliferation, cell survival, and differentiation. Takubo et al. reported that HSCs activated Pdk through HIF1α in hypoxic culture conditions, resulting in maintenance of glycolytic flow and suppression of the influx of glycolytic metabolites into mitochondria, and this glycolytic metabolic state was shown to be indispensable for the maintenance of HSCs [27]. Several studies have reported that MSCs exhibit a high level of glycolytic metabolism in the presence of high oxygen levels and further increase their rate of glycolysis on culture under hypoxia [28,29]. However, a relationship between beneficial effects of hypoxic conditions and metabolic status in addition to involvement of HIFs in the metabolic changes has not been investigated in these reports.

In this study, we aimed at investigating the effect of 5% oxygen on hADMPCs. Our results demonstrate that culture under 5% oxygen increased the glycolysis rate, improved the proliferation efficiency, prevented the cellular senescence, and maintained the undifferentiated status of hADMPCs. Intriguingly, these effects were not mediated by HIF, but rather by Notch signaling, an important signaling pathway required for the development of many cell types and maintenance of stem cells [30,31]. Five percent oxygen activated Notch signaling, resulting in the upregulation of *SLC2A3*, *TPI*, and *PGK1* in addition to the downregulation of *TIGAR* and *SCO2*, which may contribute to the increase in the glycolysis rate. These observations, thus, provide new regulatory mechanisms for stemness maintenance obtained under 5% oxygen conditions.

Materials and Methods

Adipose tissue samples

Subcutaneous adipose tissue samples (10–50 g each) were resected during plastic surgery from five female and two male patients (age 20–60 years) as discarded tissue. The study protocol was approved by the Review Board for Human Research of Kobe University Graduate School of Medicine Foundation for Biomedical Research and Innovation, Osaka City University Graduate School of Medicine, and Kinki University Pharmaceutical Research and Technology Institute (reference number: 12-043). Each subject provided signed informed consent.

Cell culture

hADMPCs were isolated as previously reported [11,32–34] and maintained in a medium containing 60% DMEM low glucose, 40% MCDB-201 medium (Sigma Aldrich), 1× insulin-transferrin-selenium (Life Technologies), 1 nM dexamethasone (Sigma Aldrich), 100 mM ascorbic acid 2-phosphate (Wako), 10 ng/mL epidermal growth factor (PeproTech), and 5% fetal bovine serum. The cells were plated to a density of 5×10^3 cells/cm^2 on fibronectin-coated dishes, and the medium was replaced every 2 days. For hypoxic culture, cells were cultured in a gas mixture composed of 90% N_2, 5% CO_2, and 5% O_2. For maintenance of the hypoxic gas mixture, a ProOx C21 carbon dioxide and oxygen controller and a C-Chamber (Biospherix) were used.

Senescence-associated β-galactosidase staining

Cells were fixed with 2% paraformaldehyde/0.2% glutaradehyde for 5 min at room temperature and then washed twice with phosphate-buffered saline (PBS). The cells were then incubated overnight at 37°C with fresh senescence-associated β-galactosidase (SA-β-Gal) chromogenic substrate solution (1 mg/mL Bluo-gal (Life Technologies), 40 mM citric acid (pH 6.0), 5 mM potassium ferrocyanide, 5 mM potassium ferricyanide, 150 mM NaCl, and 2 mM $MgCl_2$).

Measurement of ROS production

Cells were harvested and incubated with 10 μM 5-(and-6)-chloromethyl-2′,7′-dichlorodihydrofluorescein diacetate, acetyl ester (CM-H_2DCFDA). The amount of intracellular ROS production was proportional to the green fluorescence, as analyzed using a Guava EasyCyte 8HT flow cytometer (Millipore) using an argon laser at 488 nm and a 525/30 nm band pass filter, and dead cells were excluded using the Live/Dead Fixable Far Red Dead Cell Stain Kit (Life Technologies).

EdU proliferation assay

For assessment of cell proliferation, hADMPCs were seeded on a fibronectin-coated six-well plate at a density of 5×10^3 cells/cm^2 and cultured for 3 days. Cell proliferation was detected by incorporating of 5-ethynyl-2′-deoxyuridine (EdU) and using the Click-iT EdU Alexa Fluor 488 Flow Cytometry Assay Kit (Life Technologies). Briefly, according to the manufacturer's protocol, cells were incubated with 10 μM EdU for 2 h before fixation, permeabilized, and stained with EdU. EdU-positive cells were then analyzed using the 488 nm laser of a Guava EasyCyte 8HT flow cytometer (Millipore).

Flow cytometry analysis

Flow cytometry analysis was performed as previously described [34]. Briefly, hADMPCs were harvested and resuspended in staining buffer (PBS containing 1% BSA, 2 mM EDTA, and 0.01% sodium azide) at a density of

1×10^6 cells/mL, incubated for 20 min with a fluorescein isothiocyanate (FITC)-conjugated antibody against CD49b or CD98 (BioLegend) or a phycoerythrin (PE)-conjugated antibody against CD10, CD13, CD29, CD44, CD49a, CD49c, CD49d, CD49e, CD51/61, CD73, CD90, CD105, CD117, SSEA4, HLA-A,B,C (BioLegend), CD133/1 (Miltenyi Biotec), or CD166 (Beckman Coulter). Nonspecific staining was assessed using relevant isotype controls. Dead cells were excluded using the Live/Dead Fixable Far Red Dead Cell Stain Kit (Life Technologies). FlowJo software was used for quantitative analysis.

RNA extraction, cDNA generation, and quantitative polymerase chain reaction

Total RNA was extracted using the RNeasy Mini Kit (Qiagen) accroding to the manufacturer's instructions. cDNA was generated from 1 μg of total RNA using the Verso cDNA Synthesis Kit (Thermo Scientific) and purified using the MinElute PCR Purification Kit (Qiagen). Quantitative polymerase chain reaction (Q-PCR) analysis was conducted using the SsoFast EvaGreen supermix (Bio-Rad) according to the manufacturer's protocols. The relative expression value for each gene was calculated using the ΔΔCt method, and the most reliable internal control gene was determined using geNorm Software (http://medgen.ugent.be/~jvdesomp/genorm/). Details of the primers used in these experiments are available on request.

Western blot analysis

Whole cell extracts were prepared by washing cells with ice-cold PBS and lysing them with M-PER Mammalian Protein Extraction Reagent (Thermo Scientific Pierce) according to the manufacturer's instructions. Nuclear and cytosolic extracts were prepared as follows. Cells were washed with ice-cold PBS and lysed with lysis buffer (50 mM Tris-HCl (pH 7.5), 0.5% Triton X-100, 137.5 mM NaCl, 10% glycerol, 5 mM EDTA, 1 mM sodium vanadate, 50 mM sodium fluoride, 10 mM sodium pyrophosphate, and protease inhibitor cocktail). Then, insoluble nuclei were isolated by centrifugation and lysed with lysis buffer containing 0.5% SDS. Equal amounts of proteins were separated by sodium dodecyl sulfate polyacrylamide gel electrophoresis (SDS-PAGE), transferred to polyvinylidene fluoride membranes (Immobilon-P; Millipore), and probed with antibodies against cleaved Notch1 (#2421; Cell Signaling Technology), HIF-1α (#610959; BD Bioscience), hypoxia-inducible factor 2α (MAB3472; Millipore), Akt (#9272; Cell Signaling Technology), and phospho Akt (Ser473) (#4060; Cell Signaling Technology). Horseradish peroxidase (HRP)-conjugated anti-mouse or -rabbit IgG antibody (Cell Signaling Technology) was used as a secondary antibody, and immunoreactive bands were visualized using Immobilon Western Chemiluminescent HRP substrate (Millipore). The band intensity was measured using the ImageJ software.

Fluorescence microscopy

Phase-contrast and fluorescence images were obtained using a fluorescence microscope (BZ-9000; Keyence) using BZ Analyzer Software (Keyence).

Adipogenic, osteogenic, and chondrogenic differentiation procedures

For adipogenic differentiation, cells were cultured in differentiation medium (Zen-Bio). After 7 days, half of the medium was exchanged for adipocyte medium (Zen-Bio) and this was repeated every 3 days. Three weeks after differentiation, adipogenic differentiation was confirmed by a microscopic observation of intracellular lipid droplets with the aid of Oil Red O staining. Osteogenic differentiation was induced by culturing the cells in osteocyte differentiation medium (Zen-Bio). Differentiation was examined by Alizarin Red staining. For chondrogenic differentiation, 2×10^5 hADMSCs were centrifuged at 400 *g* for 10 min. The resulting pellets were cultured in chondrogenic medium (Lonza) for 21 days. The pellets were fixed with 4% paraformaldehyde in PBS, embedded in OCT, frozen, and sectioned at 8 μm. The sections were incubated with PBSMT (PBS containing 0.1% Triton X-100, and 2% skim milk) for 1 h at room temperature, and then incubated with a mouse monoclonal antibody against type II collagen (Abcam) for 1 h. After washing with PBS, cells were incubated with Alexa 546-conjugated anti-mouse IgG to identify chondrocytes (Life Technologies). The cells were counterstained with 4′-6-diamidino-2-phenylindole (DAPI) (Life Technologies) to identify cellular nuclei. The sections were also stained with 1% alcian blue (Sigma Aldrich) in 3% acetic acid, pH 2.5 for 30 min.

Determination of HK, PFK, LDH, PDH, and Cox IV activities

Cells (2×10^6) were lysed, and HK, PFK, LDH, or PDH activity was measured using the Hexokinase Colorimetric Activity Kit, Phosphofructokinase (PFK) Activity Colorimetric Assay Kit, Lactate Dehydrogenase (LDH) Activity Assay Kit, or Pyruvate Dehydrogenase Activity Colorimetric Assay Kit (all from BioVision), respectively, according to the manufacturer's instructions. To measure Cox IV activity, mitochondria were isolated from 2×10^7 cells using a Mitochondria Isolation Kit (Thermo Scientific) and lysed with buffer containing n-Dodecyl β-D-maltoside, followed by measurement with the Mitochondria Activity Assay (Cytochrome C Oxidase Activity Assay) Kit (BioChain Institute), according to the manufacturer's instructions.

Results

5% oxygen hypoxic culture condition increases proliferation capacity and decreases senescence

hADMPCs were cultured under 20% oxygen (normoxia; Nx) or 5% oxygen (hypoxia; Hx), and their proliferation capacities were examined based on the relationship between the number of cultivation days and the population doubling level (PDL). Nx-cultured hADMPCs ceased proliferation at a PDL of 35–40 (between 46–70 days), whereas continuous cell proliferation beyond 45 PDL was observed when hADMPCs were cultured in the Hx condition (Fig. 1A). To investigate whether this increase of PDL in the Hx culture condition resulted from an increase in cell cycle progression and increase in survival rates, EdU, an alternative to 5-bromo-2′-deoxyuridine (BrdU), was incorporated into the

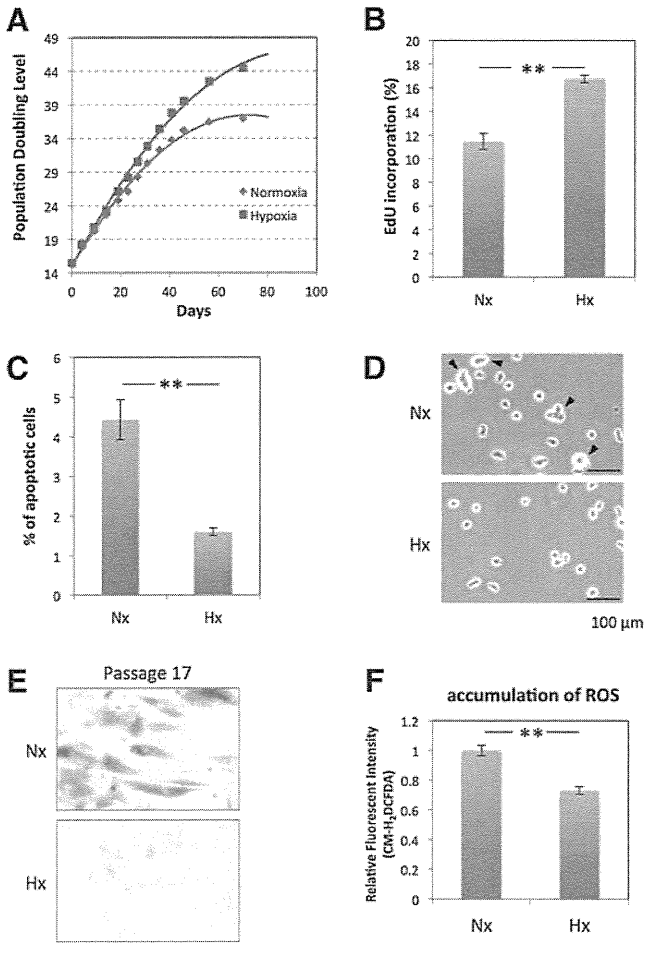

FIG. 1. Hypoxia increases proliferation capacity and decreases senescence in tissue-derived multilineage progenitor cells (hADMPCs). **(A)** Growth profiles of hADMPCs under normoxic (*red square*) and hypoxic (*blue square*) conditions. The population doubling level (PDL) was determined to be 0 when cells were isolated from human adipose tissue. Cells were maintained until they reached PDL13–15 (passage 3) and then split into four aliquots of equal cell densities. PDL was calculated based on the total cell number at each passage. **(B)** Detection of normoxic (Nx) and hypoxic (Hx) cells by flow cytometry after incorporation of EdU. **(C)** Percentages of apoptotic cells with sub-G1 DNA under Nx and Hx conditions. The results are presented as the mean of three independent experiments. **(D)** hADMPCs cultured under Nx and Hx conditions were harvested by trypsin-EDTA and then imaged using a phase-contrast microscope. *Arrowheads* indicate cells with a larger and more irregular shape. **(E)** Cells expanded under Nx and Hx conditions were stained with SA-β-gal. **(F)** Cellular reactive oxygen species detection by the oxidative stress indicator CM-H_2DCFDA in hADMPCs under Nx or Hx. Data are presented as the mean fluorescence intensity of three independent experiments. Error bars indicate SD. $^{**}P < 0.01$ indicates significant difference (independent *t*-test) between Nx and Hx. Scale bars; 100 μm. Color images available online at www.liebertpub.com/scd

genomic DNA of the hADMPCs, and the amount of incorporated EdU was quantified by flow cytometry. As shown in Fig.1B, the EdU incorporation rate was significantly higher in Hx-cultured hADMPCs than in Nx-cultured hADMPCs, suggesting that cell growth was increased in the Hx culture condition. In addition, measurement of DNA content in hADMPCs revealed a slight but significant decrease of sub-G1 peaks, which indicates the existence of apoptotic cells with degraded DNA, when the cells were cultured in the Hx condition (Fig. 1C). These data suggest that the Hx culture condition increases the proliferation capacity of hADMPCs by promoting their cell growth and survival rates. We also found that Nx-cultured hADMPCs were larger with a more irregular shape (Fig. 1D), which suggests that the Hx culture condition prevented hADMPCs from entering senescence [35]. To further investigate this phenomenon, cellular senescence was measured by staining for SA-β-Gal, which revealed that SA-β-Gal activity was increased in Nx-cultured hADMPCs at passage 17 (Fig. 1E). Since it has been hypothesized that senescence results from oxidative stress [20], accumulation of ROS in hADMPCs was detected using the nonfluorescent probe, CM-H_2DCFDA. Flow cytometry analysis revealed that ROS were generated at higher levels in hADMPCs when cultured in the Nx condition (Fig. 1F), suggesting that reduced production of ROS in the Hx condition may prevent the cells from entering replicative senescence.

Hypoxic culture maintains some MSC properties and increases differentiation

We then examined the cell properties of hADMPCs under Nx and Hx conditions. Initially, cell surface antigens expressed on hADMPCs were analyzed by flow cytometry. No significant difference in expression profile between hADMPCs cultured in Nx and Hx was observed; the cells were consistently positive for CD10, CD13, CD29, CD44, CD49a, CD49b, CD49c, CD49d, CD49e, CD51/61, CD54, CD59, CD73, CD90, CD98, CD105, CD166, and HLA-A, B, C, but negative for CD34, CD45, CD117, and CD133 (Fig. 2 and data not shown). These data were consistent with previous reports describing the expression profiles of cell surface markers of hMSCs [36,37]. To further examine the stem cell properties of hADMPCs, their potential for differentiation into adipocyte, osteocyte, and chondrocyte lineages was analyzed at passage 8. Hx-cultured hADMPCs presented enhanced differentiation into various lineages (Fig. 3A, B), indicating that the Hx culture condition improved the stem cell properties of hADMPCs.

Hypoxic culture condition activates Notch signaling

To reveal the molecular mechanism by which the Hx culture condition increased the proliferative capacity and maintained the stem cell properties of hADMPCs, we next examined Notch signaling, which is required for maintaining stem-cell features of various types of stem cells [30,31]. As expected, levels of cleaved NOTCH1, an activated form of NOTCH1, were significantly increased (greater than twofold) in the Hx culture condition (Fig. 4A). Q-PCR analysis revealed that HES1, a downstream target of Notch signaling, was upregulated in Hx-cultured hADMPCs, which also indicated that Notch signaling was activated in

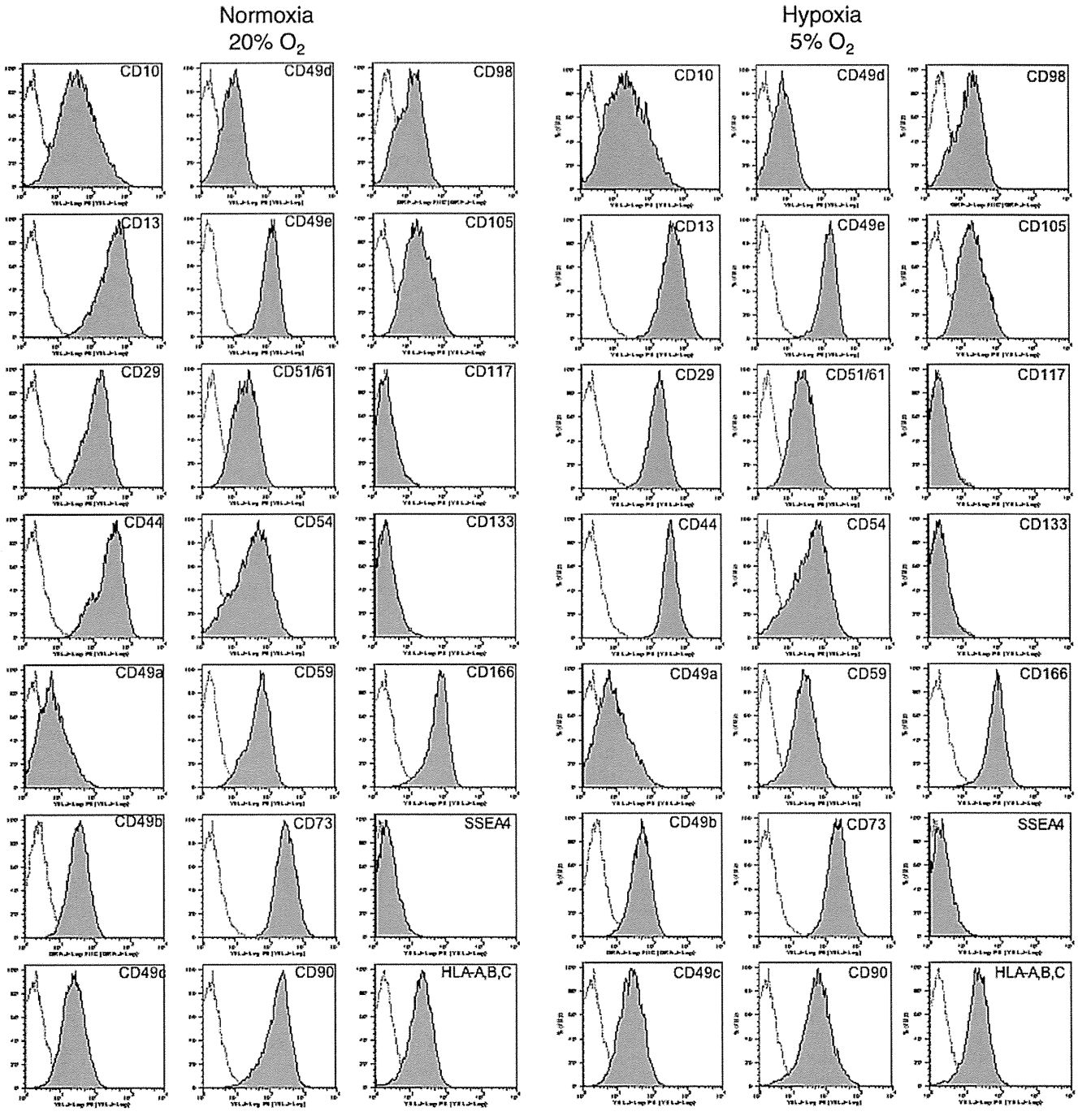

FIG. 2. Hypoxic culture maintains mesenchymal stem cell properties. hADMPCs cultured under normoxia (20% O_2) or hypoxia (5% O_2) were labeled with antibodies against the indicated antigens and analyzed by flow cytometry. Representative histograms are shown. The respective isotype control is shown as a *gray line*.

the Hx culture condition (Fig. 4B). Administration of the γ-secretase inhibitor DAPT at 1 μM, which was sufficient to inhibit the proteolytic cleavage of NOTCH1 (Fig. 4A), decreased the Hx-induced expression of HES1 at both mRNA and protein levels (Fig. 4B, C). These data indicate that Hx increased the expression of HES1 through activation of Notch signaling. It has been reported that Notch signaling and hypoxia-inducible factor (HIF) undergo crosstalk in hypoxic cells [38–41]. Therefore, HIF-1α and HIF-2α protein levels in hADMPCs were analyzed by western blotting. HIF-1α was stabilized when a chemical hypoxia-mimicking agent, cobalt chloride, was applied in the culture; whereas no obvious increase of HIF-1α was observed in the Hx culture condition (Fig. 4D). However, we did not detect any HIF-2α expression even in the presence of cobalt chloride (Fig. 4E). Q-PCR analysis revealed that *HIF2A* mRNA was not expressed in these cells (data not shown). From these results, we concluded that neither HIF-1α nor HIF-2α was involved in the Hx-induced increase in the proliferative capacity and stem cell properties of hADMPCs.

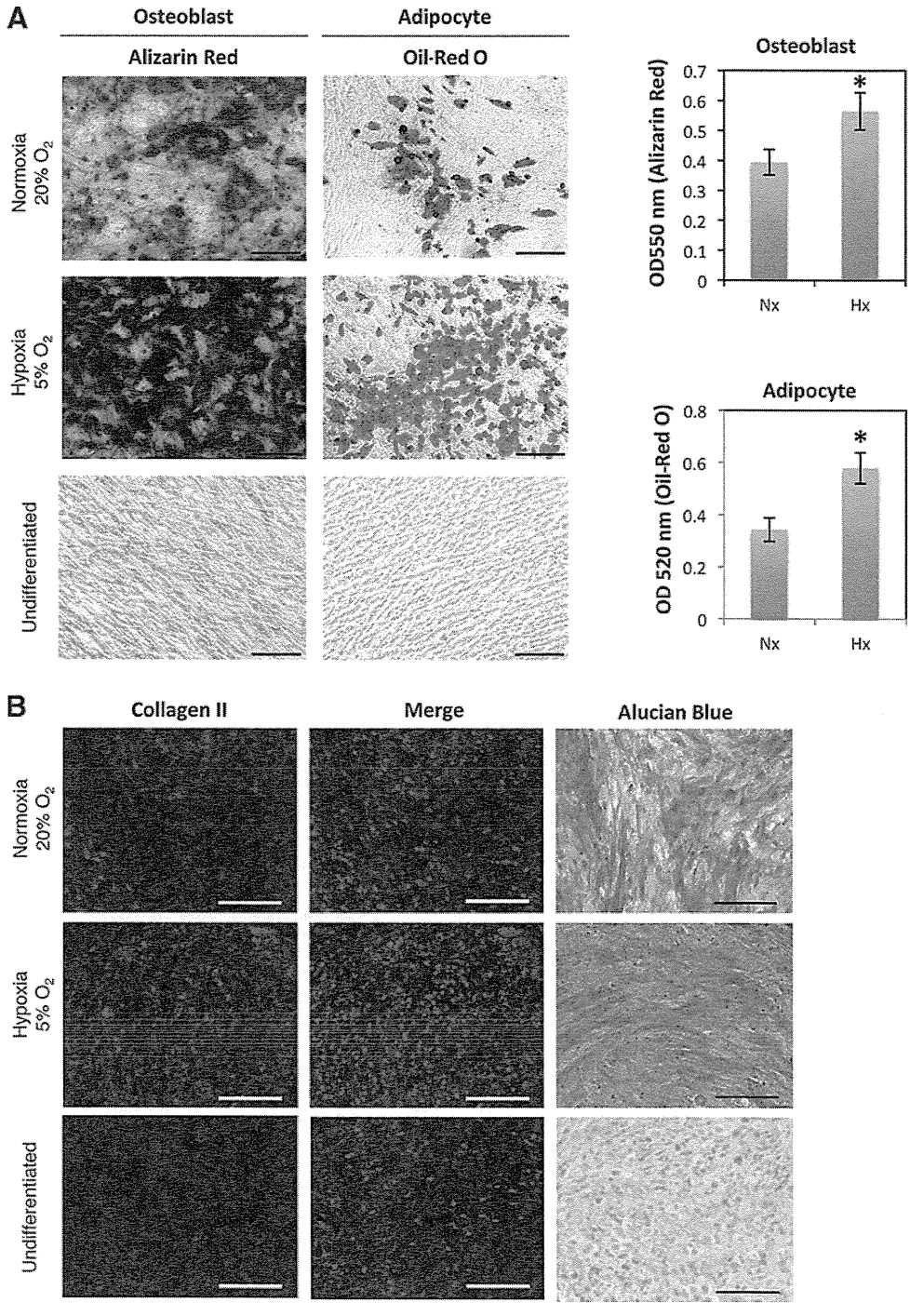

FIG. 3. Hypoxic culture enhances stem cell properties. hADMPCs were expanded under normoxic and hypoxic conditions. **(A)** Normoxic (20% O_2) and hypoxic (5% O_2) cells at passage 8 were induced for 3 weeks to differentiate into osteoblasts and adipocytes and stained with Alizarin Red and Oil-Red O, respectively. The stained dye was extracted, and OD values were measured and plotted as the means of three independent experiments ± SD. $^*P < 0.05$. Scale bars, 200 μm. **(B)** Normoxic (20% O_2) and hypoxic (5% O_2) cells at passage 8 were induced for 3 weeks to differentiate to chondrocytes, and immunofluorescent analysis of collagen II (*red*) and Alucian Blue staining were performed. The *blue* signals indicate nuclear staining. Scale bars, 100 μm. Non-induced control cultures in growth medium without adipogenic, osteogenic or chondrogenic differentiation stimuli are shown (Undifferentiated). Color images available online at www.liebertpub.com/scd

To identify the signaling responsible for the observed effect, we next examined the Akt, NF-κB, and p53 signaling pathways. It has been reported that hypoxic conditions induce the activation of Akt and NF-κB signaling [42,43]. In addition, hypoxic conditions have been shown to inhibit p53 activity [44], and crosstalk between these pathways and Notch signaling has also been demonstrated [41,45–47]. As shown in Fig. 4F, the Hx condition increased Akt phosphorylation, which was not decreased by DAPT treatment. These data demonstrate that 5% oxygen activated Akt signaling but not via Notch signaling. Similarly, the hypoxic condition induced nuclear accumulation of p65, which was inhibited by DAPT treatment (Fig. 4G). These data suggest that NF-κB signaling is regulated by Notch signaling in hADMPCs. Furthermore, p53 was not activated under the 5% oxygen condition as assessed by detection of phospho-p53 and a p53 reporter assay. However, DAPT treatment significantly increased p53 activity (Fig. 4H, I).

Notch signaling is indispensable for acquisition of the advantageous properties of hADMPCs

We next examined the roles of Notch signaling in the proliferative capacity and stem cell properties of hADMPCs

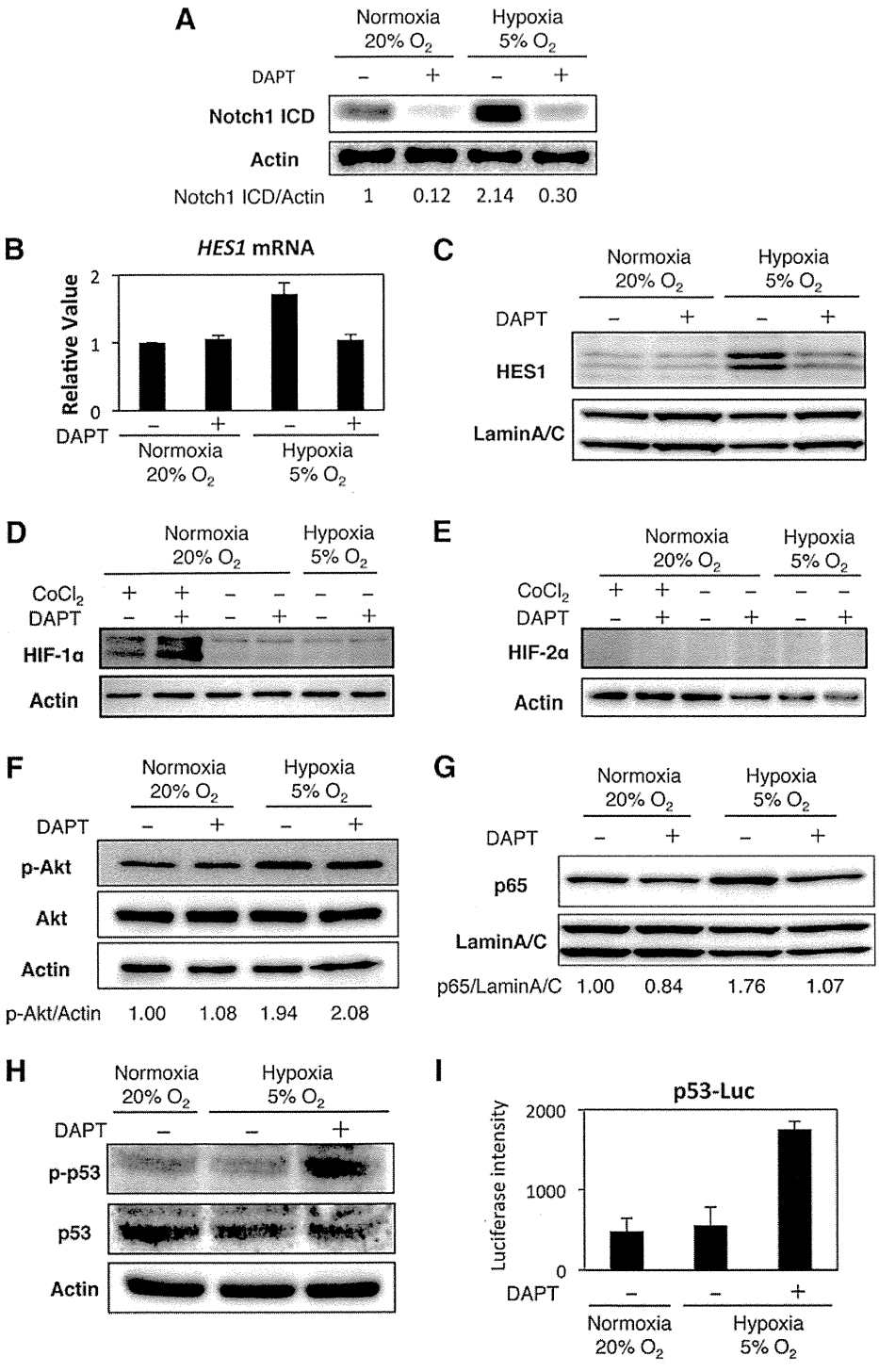

FIG. 4. Hypoxic culture condition activates Notch signaling but not HIF proteins. hADMPCs were expanded under normoxic (20% O_2) and hypoxic (5% O_2) conditions. DAPT (1 μM) was added to inhibit Notch signaling. **(A)** Western blot analysis of intracellular domain of Notch1 (Notch1 ICD) expression. Actin served as the loading control. Numbers below blots indicate relative band intensities as determined by ImageJ software. **(B)** Q-PCR analysis of *HES1*. Each expression value was calculated with the ΔΔCt method using *UBE2D2* as an internal control. **(C)** Western blot analysis of HES1 in nuclear fractions of hADMPCs. Lamin A/C served as the loading control. **(D, E)** Western blot analysis of HIF-1α **(D)** and HIF-2α **(E)**. Cobalt chloride ($CoCl_2$) was added at a concentration of 100 μM to stabilize HIF proteins (positive control). **(F)** Western blot analysis of phosphorylated Akt (p-Akt) and Akt. Actin served as the loading control. Numbers below blots indicate relative band intensities as determined by ImageJ software. **(G)** Western blot analysis of nuclear localization of p65. Lamin A/C served as the loading control. Numbers below blots indicate relative band intensities as determined by ImageJ software. **(H)** Western blot analysis of phosphorylated p53 (p-p53) and p53. Actin served as the loading control. **(I)** Activity of p53 was measured by the p53-luciferase reporter assay. Relative luciferase activity was determined from three independent experiments and normalized to pGL4.74 activity.

in the Hx culture condition. To inhibit Notch signaling, DAPT was added to the medium at a final concentration of 1 μM. DAPT treatment significantly decreased the PDL when hADMPCs were cultured under either 20% or 5% oxygen (Fig. 5A). Intriguingly, measurement of the DNA content in hADMPCs revealed that inhibition of Notch signaling by 1 μM DAPT significantly attenuated the decrease in apoptotic cells in the Hx condition (Fig. 5B). These data suggest that 5% oxygen increases the proliferation capacity of hADMPCs through Notch signaling by promoting their survival. To examine whether Notch signaling affects the stem cell properties of hADMPCs, differentiation into adipocyte, osteocyte, and chondrocyte lineages was analyzed at passage 8. Hx-cultured hADMPCs underwent greater differentiation into all lineages as described in Fig. 3, whereas application of a Notch inhibitor significantly decreased the differentiation capacity to all lineages (Fig. 5C–E). In addition, SA-β-Gal staining revealed that inhibition of Notch signaling by DAPT remarkably promoted senescence in both the Nx and Hx

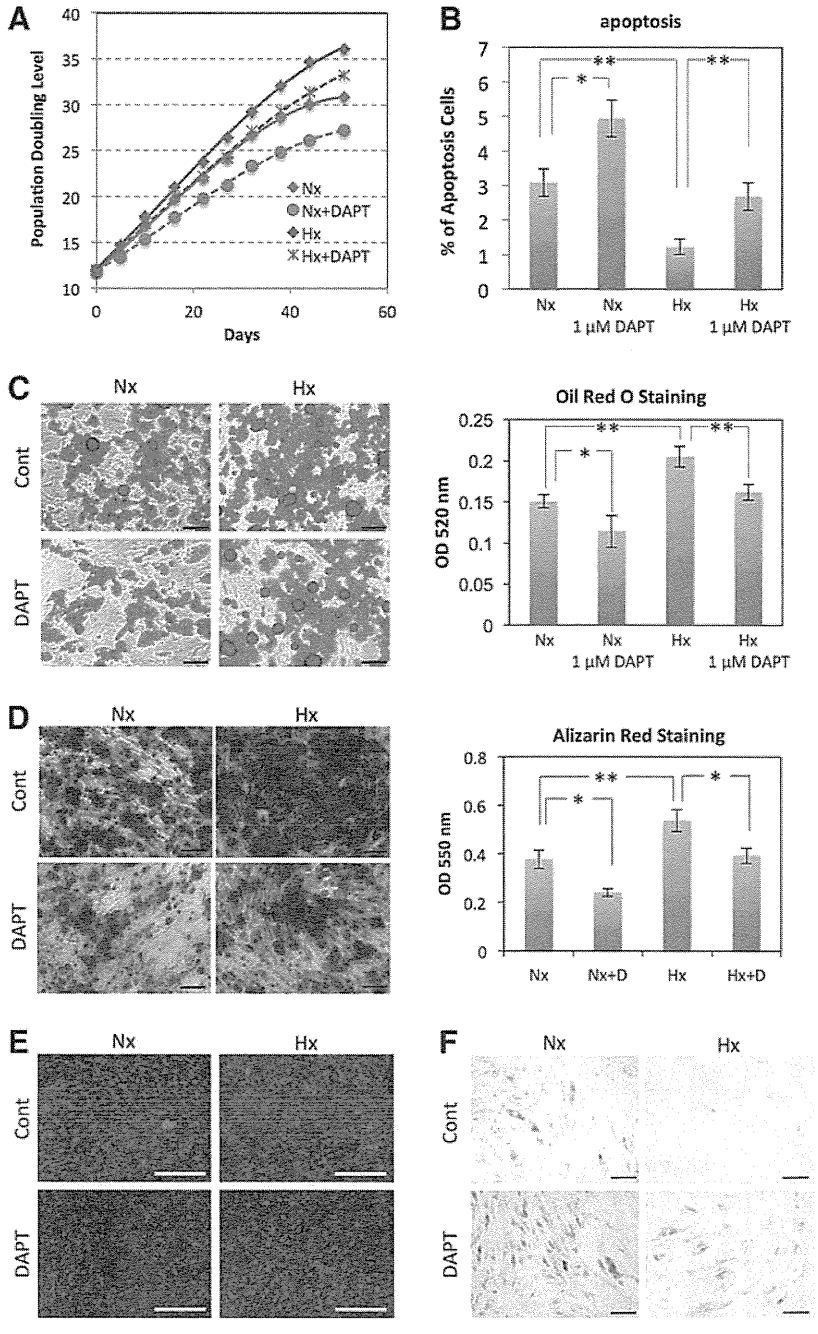

FIG. 5. Notch signaling is indispensable for acquisition of the advantageous properties of hADMPCs. hADMPCs were expanded under normoxic (20% O_2; Nx) and hypoxic (5% O_2; Hx) conditions. DAPT (1 μM) was added to inhibit Notch signaling. **(A)** Growth profiles of hADMPCs under Nx (*red*) and Hx (*blue*) conditions. *Solid lines* represent control cells, and *dotted lines* represent DAPT-treated cells. The number of population doublings was calculated based on the total cell number at each passage. **(B)** Percentages of apoptotic cells with sub-G1 DNA. Results are presented as the mean of three independent experiments ± SD. **(C, D)** hADMPCs at passage 8 were induced for 3 weeks to differentiate into adipocytes **(C)** and osteoblasts **(D)** and stained with Oil Red O and Alizarin Red, respectively. The stained dye was extracted, and OD values were measured and plotted as the means of three independent experiments ± SD. **(E)** hADMPCs at passage 8 were induced for 3 weeks to differentiate into chondrocytes, and an immunofluorescent analysis of collagen II (*red*) was performed. The *blue* signals indicate nuclear staining. **(F)** hADMPCs were stained with SA-β-gal. $*P<0.05$ and $**P<0.01$ indicate significant differences (independent *t*-test) between Nx and Hx. Scale bars; 100 μm. Color images available online at www.liebertpub.com/scd

culture conditions, suggesting that the suppression of replicative senescence observed in the Hx condition is mediated by Notch signaling (Fig. 5F).

Glycolysis is enhanced in the 5% oxygen condition through Notch signaling

Recent studies suggest that the metabolic shift from aerobic mitochondrial respiration to glycolysis extends the life span possibly via reduction of intrinsic ROS production [18,19]. Our results demonstrate that the 5% oxygen condition reduced ROS accumulation in hADMPCs (Fig. 1F). In addition, the relationship between Notch signaling and glycolysis has been recently established [48,49]. We, therefore, considered glycolytic flux by measuring the glucose consumption and lactate production of hADMPCs in the Nx or Hx culture conditions. As shown in Fig. 6A, glucose consumption and lactate production were elevated in the Hx culture condition, indicating that a metabolic shift to glycolysis occurred when hADMPCs were cultured in 5% oxygen. In contrast, the Notch inhibitor DAPT markedly reduced glycolytic flux as assessed by glucose consumption and lactate production (Fig. 6A). To identify the genes responsible for the glycolytic change, we performed a Q-PCR analysis. As shown in Fig. 6B, *SLC2A3, TPI, and PGK1*, encoding glycolytic enzymes, were upregulated in the 5% oxygen condition; whereas these genes were suppressed by DAPT treatment. Interestingly, Hes1 transduction by an adenoviral vector markedly induced the mRNA expression of the same genes (Fig. 6E). In addition, SCO2, a positive

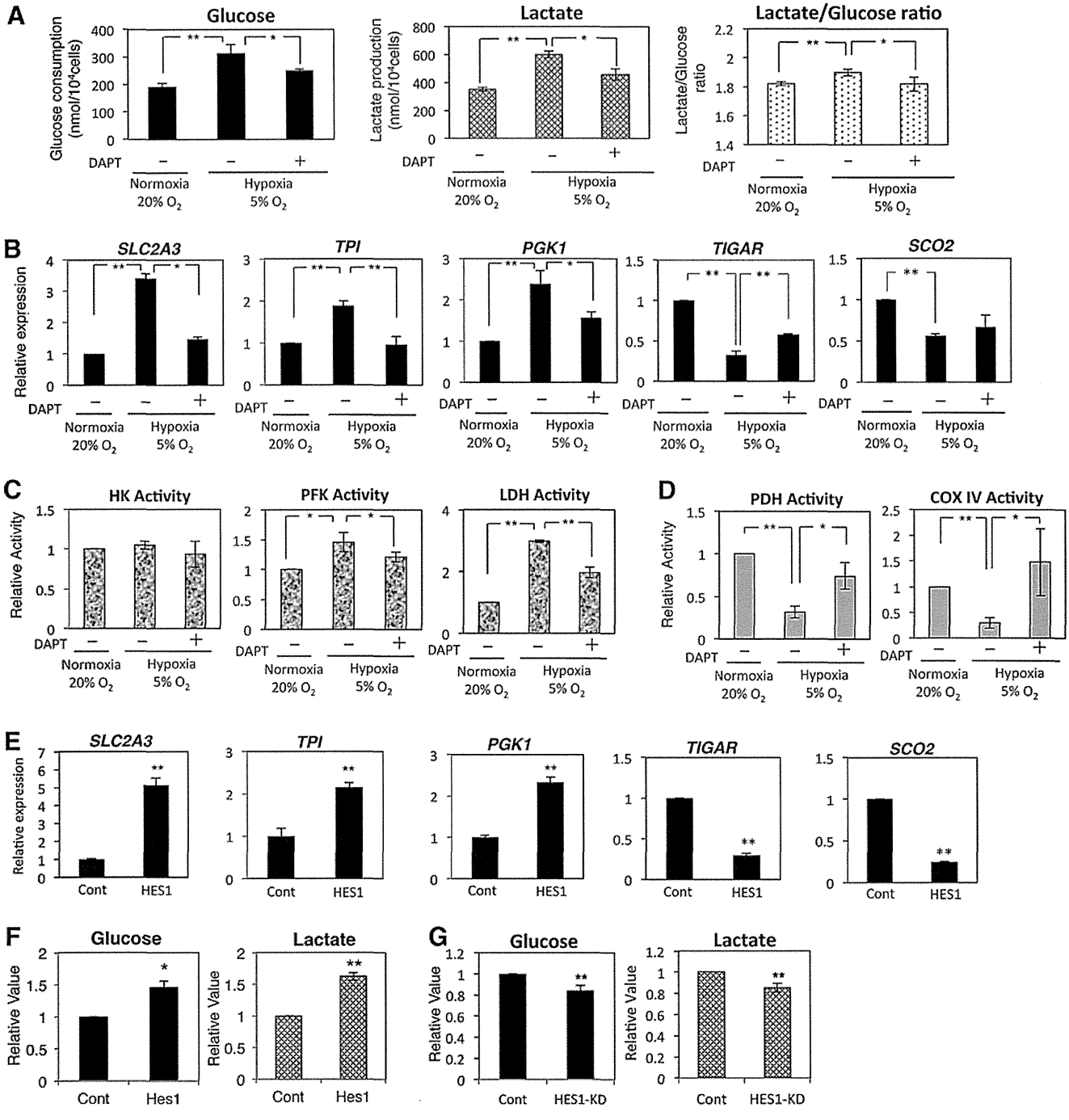

FIG. 6. Glycolysis is enhanced under 5% oxygen through Notch signaling. (**A–D**) hADMPCs were expanded under normoxic (20% O_2) and hypoxic (5% O_2) conditions. DAPT (1 μM) was added to inhibit Notch signaling. (**A**) Glucose consumption and lactate production of hADMPCs were measured and plotted as the means of three independent experiments ± SD. (**B**) Relative mRNA expression of *SLC2A3*, *TPI*, *PGK1*, *TIGAR*, and *SCO2* in hADMPCs. Each expression value was calculated with the ΔΔCt method using *UBE2D2* as an internal control. (**C, D**) Hexokinase (HK), phosphofructokinase (PFK), lactate dehydrogenase (LDH) (**C**), pyruvate dehydrogenase (PDH), and Complex IV (Cox IV) (**D**) activities were measured and the value of relative activity was plotted as the means of three independent experiments ± SD. (**E, F**) hADMPCs were transduced with either mock (Cont) or HES1 and then cultured for 3 days. (**E**) Relative mRNA expression of *SLC2A3*, *TPI*, *PGK1*, *TIGAR*, and *SCO2* in hADMPCs. Each expression value was calculated with the ΔΔCt method using *UBE2D2* as an internal control. (**F**) Glucose consumption and lactate production of hADMPCs were measured and plotted as the means of three independent experiments ± SD. (**G**) hADMPCs were transduced with either scrambled control RNAi (Cont) or RNAi against HES1 (HES1-KD), and then cultured for 3 days. Glucose consumption and lactate production of hADMPCs were measured and plotted as the means of three independent experiments ± SD. $^{**}P < 0.01$. $^{*}0.01 < P < 0.05$.

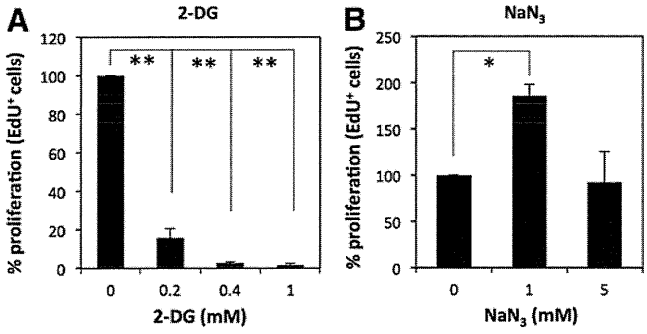

FIG. 7. Glycolysis supports proliferation of hADMPCs. hADMPCs were treated with 0, 0.2, 0.4, and 1 mM 2-deoxy-D-glucose (2-DG) **(A)** or 0, 1, and 5 mM sodium azide (NaN_3) **(B)** for 24 h. Cells were then allowed to incorporate EdU for 2 h, and the EdU-positive cells were analyzed by flow cytometry. The percentages for the 0 mM control were plotted as the means of three independent experiments ± SD. $^*P < 0.05$; $^{**}P < 0.01$.

modulator of aerobic respiration, and TIGAR, a negative regulator of glycolysis, were transcriptionally downregulated in the 5% oxygen condition; whereas DAPT treatment partially restored the expression level (Fig. 6B). Adenoviral expression of Hes1 dramatically reduced *SCO2* and *TIGAR* expression (Fig. 6E), which suggests that the Notch-Hes1 signaling modulates the metabolic pathway. We also measured the activities of key enzymes in glycolysis. Hexokinase activity was not changed under hypoxic conditions; however, PFK and LDH were activated in 5% oxygen condition, which was attenuated by Notch inhibition (Fig. 6C). In addition, pyruvate dehydrogenase (PDH) and cytochrome c oxidase (Complex IV) activity assays showed that mitochondrial respiration decreased under the hypoxic condition and that DAPT treatment restored it (Fig. 6D). Moreover, glycolytic flux in Hes1-expressing hADMPCs was positively correlated with the expression of these glycolytic genes as assessed by glucose consumption and lactate production (Fig. 6F). In contrast, HES1 knockdown by adenoviral transduction of *HES1* RNAi resulted in a significant reduction of glycolytic flux (Fig. 6G), demonstrating that HES1 is involved in the regulation of glycolysis.

Glycolysis supports the proliferation of hADMPCs

To determine whether aerobic glycolysis is important for the proliferation of hADMPCs, hADMPCs were treated with the glycolytic inhibitor 2-deoxy-D-glucose (2-DG) or the respiration inhibitor sodium azide (NaN_3). We found that hADMPCs were sensitive to treatment with 2-DG even at a low concentration of 0.2 mM (Fig. 7A). In contrast, treatment of hADMPCs with NaN_3 rather increased their proliferation at the concentration of 1 mM and supported their proliferation even at the concentration of 5 mM (Fig. 7B). These data suggest that the proliferation of hADMPCs is compromised when aerobic glycolysis is blocked.

Discussion

Recent evidence suggests that hypoxic culture conditions confer a growth advantage, prevent premature senescence, and maintain undifferentiated states in ESCs, iPSCs, and somatic stem cells. However, the molecular mechanism underlying the beneficial effects of culturing these cells at low oxygen conditions remains unclear. Our findings prompted us to hypothesize that Notch signaling in physiological hypoxic conditions (5% O_2) contributes to these effects on hADMPCs by modulating glycolytic flux.

We found that 5% O_2 significantly increased the proliferation capacity, decreased apoptosis, and inhibited senescence of hADMPCs (Fig. 1). Moreover, 5% O_2 improved the differentiation of hADMPCs without affecting the expression of their cell surface markers (Figs. 2 and 3). Welford et al. reported that HIF-1α delays premature senescence of mouse embryonic fibroblasts under hypoxic conditions (2% O_2) [50]. Tsai et al. reported that hypoxia (1% O_2) inhibits senescence and maintains MSC properties through accumulation of HIF-1α [26]. Hypoxia was recently reported to enhance the undifferentiated status and stem cell properties in various stem and precursor cell populations via the interaction of HIF with the Notch intracellular domain to activate Notch-responsive promoters [38]. In the current study, the effects observed in 5% O_2 condition were independent of HIF proteins, because accumulation of HIF-1α and HIF-2α was not observed (Fig. 4). Instead, our findings suggest that 5% O_2 activated Notch signaling, which contributed advantageous effects of hypoxic culture on hADMPCs. A pharmacological inhibitor of Notch signaling, DAPT, abrogated the hypoxic-induced Notch activation, increased proliferation capacity and lifespan, maintenance of stem cell properties, and prevention of senescence (Figs. 4 and 5). Moreover, we also found that 5% O_2 enhanced glucose consumption and lactate production, and these effects were also attenuated by Notch inhibition (Fig. 6A) and knockdown of HES1 (Fig. 6G). Previously, it has been reported that Notch signaling promotes glycolysis by activating the PI(3)K-Akt pathway [48,49]. However, our results indicate that Akt signaling was not activated by Notch signaling, because DAPT did not attenuate hypoxia-induced Akt phosphorylation (Fig. 4F). Although Akt is unlikely to be regulated by Notch signaling in hADMPCs, it is obvious in our data that Akt signaling was activated by 5% O_2. Therefore, we could not rule out the possibility that the promotion of glycolysis in the 5% O_2 condition was caused by Akt signaling.

Recent evidence suggests that Notch signaling acts as a metabolic switch [48,51]. Zhou et al. demonstrated that hairy, a basic helix-loop-helix transcriptional repressor regulated by Notch signaling, was upregulated and genes encoding metabolic enzymes, including TCA cycle enzymes and respiratory chain complexes, were downregulated in hypoxia-tolerant flies. Intriguingly, they also found that hairy-binding elements were present in the regulatory region of the downregulated metabolic genes. Their work, thus, provides new evidence that hairy acts as a metabolic switch [51]. Landor et al. demonstrated that both hyper- and hypoactive Notch signaling induced glycolysis, albeit by different mechanisms. They showed that Notch activation increased glycolysis through activation of PI3K-AKT signaling, whereas decreased Notch activity inhibited mitochondrial function in a p53-dependent manner in MCF7 breast cancer cell lines [48]. Consistent with their reports, our findings that Notch signaling promoted activity of some glycolysis enzymes and inhibited mitochondrial activity

(Fig. 6) also suggest that Notch signaling functioned as a metabolic switch. While our data showed that Notch inhibition by DAPT resulted in reduced glycolysis (Fig. 6A–C), induction of mitochondrial function (Fig. 6D) and activation of p53 (Fig. 4H, I) are not consistent with the report of Landor el al. This contradiction might be explained by the expression level of endogenous Notch. Landor et al. showed that in breast cancer MDA-M-231 cells, which showed higher endogenous Notch activity, high glucose uptake, and lactate production than MCF7 breast cancer cell lines, Notch inhibition by DAPT significantly reduced glucose consumption and lactate production [48]. As shown in Fig. 4A, we observed that hADMPCs in 5% O_2 displayed high Notch activity. Moreover, the lactate-to-glucose ratio was 1.8–1.9 in hADMPCs, suggesting that hADMPCs largely rely on glycolysis for energy production (Fig. 6A). In addition, it was reported that hMSCs showed a higher glycolytic rate than primary human fibroblast [52]. It appears that hADMPCs cultured under hypoxic conditions might possess cell properties similar to MDA-M-231 cells or MCF7 cells, in which stable expression of constructs NICD1-GFP produces high Notch activity.

Nuclear translocation of p65 was observed in hypoxic conditions, demonstrating that NF-κB is a direct target of Notch signaling (Fig. 4G). Intriguingly, the hypoxic culture conditions in this study upregulated several genes encoding glycolytic enzymes (*SLC2A3, TPI, and PGK1*); whereas the expression of these genes was suppressed by Notch inhibition. In addition, Hes1 transduction induced mRNA expression of the same genes (Fig. 6). It was previously reported that *SLC2A3* expression was regulated by p65/NF-κB signaling, and that Notch/Hes1 is able to induce the activation of the NF-κB pathway in human T-ALL lines and animal disease models [53]. Espinosa et al. demonstrated that Hes1 directly targeted the deubiquitinase CYLD, resulting in deubiquitination and inactivation of TAK1 and IKK, degradation of IκBa, and activation of NF-κB signaling [53]. In our systems, however, we did not observe repression of *CYLD* mRNA in Hes1-overexpressing hADMPCs (data not shown). While *PGK1* mRNA has been reported to be upregulated by NF-κB, it has not clearly been shown to be controlled by NF-κB despite the presence of an NF-κB site in the promoter [54]. Although modulation of *TPI* expression by NF-κB has not been reported, we found several NF-κB binding sites on the human *TPI* promoter (data not shown). Since NF-κB is likely to be one of the responsible signals for hypoxic-induced glycolysis [53], further analysis will be required to determine the mechanism by which NF-κB signaling is induced by Notch signaling. In addition, it will be important to investigate whether NF-κB is really responsible for the observed glycolysis and whether it regulates the expression of *SLC2A3*, *TPI*, and *PGK1* in hADMPCs under 5% oxygen.

In addition, SCO2, a positive modulator of aerobic respiration, and TIGAR, a negative regulator of glycolysis, were transcriptionally downregulated in the 5% oxygen condition; whereas DAPT treatment partially restored expression (Fig. 6B). We observed some glycolysis and mitochondrial enzyme activity and found that the activities of COX IV and PFK were consistent with gene expression data (Fig. 6C, D). Adenoviral expression of Hes1 dramatically reduced *SCO2* and *TIGAR* expression (Fig. 6E), which suggests that Notch-Hes1 signaling modulates the metabolic pathway. Intriguingly, our results also indicate that Hes1 could suppress the expression of *TIGAR* and *SCO2*, a p53 target gene. It has been reported that Notch signaling suppresses p53 in lymphomagenesis [46]. Moreover, Kim et al. reported that NICD1 inhibits p53 phosphorylation and represses p53 transactivation by interacting with p53 [47]. In addition, DAPT treatment resulted in the enhancement of p53 activity in the hypoxic conditions (Fig. 4H, I). Therefore, it is possible that p53 activation was regulated by Notch signaling in hADMPCs, although we did not observe a decrease in p53 activity in hypoxic conditions in this study (Fig. 4). Further analysis will be required to determine whether p53 activity is suppressed in hypoxic conditions over a longer period of culture.

Cells undergoing active proliferation utilize large amounts of glucose through glycolysis, producing pyruvate for use in substrates (amino acids and lipids) and the pentose shunt for use in nucleic acid substrates, and also producing NADPH as a reducing agent to counter oxidative stress [18,55]. In the current study, 5% O_2 actually increased proliferation and decreased the accumulation of ROS, which may be involved in the reduction of senescence (Fig. 1). Since accumulation of endogenous ROS might be a major reason for replicative senescence [20], enhancing glycolysis in cultured cells may improve the quality of the cells by suppressing premature senescence. Kondoh et al. demonstrated that enhanced glycolysis is involved in cellular immortalization through reduction of intrinsic ROS production [14,18,19]. Therefore, it is possible that the extension of lifespan observed in our experimental conditions was caused by the reduction of intracellular ROS levels through enhanced glycolysis by Notch signaling. Our data indicate that aerobic glycolysis is utilized for proliferation of hADMPCs, because the glycolytic inhibitor 2-DG attenuates the proliferation rate of hADMPCs (Fig. 7A). Intriguingly, the aerobic respiration block by NaN_3 did not decrease the proliferation; rather, it increased proliferation at a low concentration (Fig. 7B), which may support our data indicating that the metabolic switch from mitochondrial respiration to glycolysis provides a growth advantage to hADMPCs. However, the question of whether the enhanced glycolysis really contributes to the prolonged lifespan in hADMPCs remains to be determined in this study.

In the current study, the molecular mechanism for how Notch signaling is activated in 5% O_2 conditions was explored. It has been reported that Notch1 activity is influenced by oxygen concentration [40,41,56]. In melanoma cells, hypoxia (2% O_2) resulted in increased expression of Notch1 by HIF-1α and also by Akt through NF-κB activity [41]. Similarly, in hypoxic breast cancer cells, Notch ligand JAG2 was shown to be transcriptionally activated by hypoxia (1% O_2) in an HIF-1α-dependent manner, resulting in an elevation of Notch signaling [40]. In contrast, in hESCs continuously cultured in 5% O_2, alteration of the Notch pathway seems to be independent of HIF-1α [56]. In our system, Notch1 activation was not likely dependent on HIF-1α and HIF-2α, because these proteins did not accumulate in the Hx condition. In contrast, our results indicate that the 5% O_2 condition activated Akt and NF-κB signaling (Fig. 4), which suggests that these molecules may activate Notch signaling in hADMPCs. NF-κB was previously shown to

increase Notch1 activity indirectly by increasing the expression of Notch ligand Jagged1 in HeLa, lymphoma, and myeloma cells [57]. In addition, Akt regulated Notch1 by increasing Notch1 transcription through the activity of NF-κB in melanoma cells [41]. Further analysis is required to clarify the mechanism underlying this phenomenon.

In conclusion, the 5% oxygen condition conferred a growth advantage through a metabolic shift to glycolysis, improved the proliferation efficiency, prevented the cellular senescence, and maintained the undifferentiated status of hADMPCs. These observations, thus, provide new regulatory mechanisms for the maintenance of stemness observed in 5% oxygen conditions. In addition, our study sheds new light on the regulation of replicative senescence, which might have an impact for quality control of hADMPC preparations used for therapeutic applications.

Acknowledgments

The authors would like to thank Koichi Sakaguchi, Mio Oishi, Mika Uemura, and Kei Sawaragi for technical support. This work was supported by MEXT KAKENHI grant number 24791927 to H.M. This work was also supported in part by grants from the Ministry of Health, Labor, and Welfare of Japan and a grant from the Program for Promotion of Fundamental Studies in Health Sciences of the National Institute of Biomedical Innovation (NIBIO).

Author Disclosure Statement

The authors declare no conflict of interest. No competing financial interests exist.

References

1. Okura H, H Komoda, A Saga, A Kakuta-Yamamoto, Y Hamada, Y Fumimoto, CM Lee, A Ichinose, Y Sawa and A Matsuyama. (2010). Properties of hepatocyte-like cell clusters from human adipose tissue-derived mesenchymal stem cells. Tissue Eng Part C Methods 16:761–770.
2. Okura H, A Matsuyama, CM Lee, A Saga, A Kakuta-Yamamoto, A Nagao, N Sougawa, N Sekiya, K Takekita, et al. (2010). Cardiomyoblast-like cells differentiated from human adipose tissue-derived mesenchymal stem cells improve left ventricular dysfunction and survival in a rat myocardial infarction model. Tissue Eng Part C Methods 16:417–425.
3. Okura H, H Komoda, Y Fumimoto, CM Lee, T Nishida, Y Sawa and A Matsuyama. (2009). Transdifferentiation of human adipose tissue-derived stromal cells into insulin-producing clusters. J Artif Organs 12:123–130.
4. Safford KM, SD Safford, JM Gimble, AK Shetty and HE Rice. (2004). Characterization of neuronal/glial differentiation of murine adipose-derived adult stromal cells. Exp Neurol 187:319–328.
5. Leu S, YC Lin, CM Yuen, CH Yen, YH Kao, CK Sun and HK Yip. (2010). Adipose-derived mesenchymal stem cells markedly attenuate brain infarct size and improve neurological function in rats. J Transl Med 8:63.
6. Ikegame Y, K Yamashita, S Hayashi, H Mizuno, M Tawada, F You, K Yamada, Y Tanaka, Y Egashira, et al. (2011). Comparison of mesenchymal stem cells from adipose tissue and bone marrow for ischemic stroke therapy. Cytotherapy 13:675–685.
7. Tan B, Z Luan, X Wei, Y He, G Wei, BH Johnstone, M Farlow and Y Du. (2011). AMP-activated kinase mediates adipose stem cell-stimulated neuritogenesis of PC12 cells. Neuroscience 181:40–47.
8. Reid AJ, M Sun, M Wiberg, S Downes, G Terenghi and PJ Kingham. (2011). Nerve repair with adipose-derived stem cells protects dorsal root ganglia neurons from apoptosis. Neuroscience 199:515–522.
9. Rehman J, D Traktuev, J Li, S Merfeld-Clauss, CJ Temm-Grove, JE Bovenkerk, CL Pell, BH Johnstone, RV Considine and KL March. (2004). Secretion of angiogenic and antiapoptotic factors by human adipose stromal cells. Circulation 109:1292–1298.
10. Lee EY, Y Xia, WS Kim, MH Kim, TH Kim, KJ Kim, BS Park and JH Sung. (2009). Hypoxia-enhanced wound-healing function of adipose-derived stem cells: increase in stem cell proliferation and up-regulation of VEGF and bFGF. Wound Repair Regen 17:540–547.
11. Moriyama M, H Moriyama, A Ueda, Y Nishibata, H Okura, A Ichinose, A Matsuyama and T Hayakawa. (2012). Human adipose tissue-derived multilineage progenitor cells exposed to oxidative stress induce neurite outgrowth in PC12 cells through p38 MAPK signaling. BMC Cell Biol 13:21.
12. Wu H, Z Ye and RI Mahato. (2011). Genetically modified mesenchymal stem cells for improved islet transplantation. Mol Pharm 8:1458–1470.
13. Wagner W, P Horn, M Castoldi, A Diehlmann, S Bork, R Saffrich, V Benes, J Blake, S Pfister, V Eckstein and AD Ho. (2008). Replicative senescence of mesenchymal stem cells: a continuous and organized process. PLoS One 3: e2213.
14. Kondoh H, ME Lleonart, Y Nakashima, M Yokode, M Tanaka, D Bernard, J Gil and D Beach. (2007). A high glycolytic flux supports the proliferative potential of murine embryonic stem cells. Antioxid Redox Signal 9:293–299.
15. Prigione A, B Fauler, R Lurz, H Lehrach and J Adjaye. (2010). The senescence-related mitochondrial/oxidative stress pathway is repressed in human induced pluripotent stem cells. Stem Cells 28:721–733.
16. Varum S, AS Rodrigues, MB Moura, O Momcilovic, C At Easley, J Ramalho-Santos, B Van Houten and G Schatten. (2011). Energy metabolism in human pluripotent stem cells and their differentiated counterparts. PLoS One 6:e20914.
17. Warburg O, F Wind and E Negelein. (1927). The Metabolism of tumors in the body. J Gen Physiol 8:519–530.
18. Kondoh H. (2008). Cellular life span and the Warburg effect. Exp Cell Res 314:1923–1928.
19. Kondoh H, ME Lleonart, J Gil, J Wang, P Degan, G Peters, D Martinez, A Carnero and D Beach. (2005). Glycolytic enzymes can modulate cellular life span. Cancer Res 65: 177–185.
20. Beckman KB and BN Ames. (1998). The free radical theory of aging matures. Physiol Rev 78:547–581.
21. Ezashi T, P Das and RM Roberts. (2005). Low O2 tensions and the prevention of differentiation of hES cells. Proc Natl Acad Sci U S A 102:4783–4788.
22. Forristal CE, KL Wright, NA Hanley, RO Oreffo and FD Houghton. (2010). Hypoxia inducible factors regulate pluripotency and proliferation in human embryonic stem cells cultured at reduced oxygen tensions. Reproduction 139:85–97.
23. Yoshida Y, K Takahashi, K Okita, T Ichisaka and S Yamanaka. (2009). Hypoxia enhances the generation of induced pluripotent stem cells. Cell Stem Cell 5:237–241.

24. Takubo K, N Goda, W Yamada, H Iriuchishima, E Ikeda, Y Kubota, H Shima, RS Johnson, A Hirao, M Suematsu and T Suda. (2010). Regulation of the HIF-1alpha level is essential for hematopoietic stem cells. Cell Stem Cell 7:391–402.
25. Santilli G, G Lamorte, L Carlessi, D Ferrari, L Rota Nodari, E Binda, D Delia, AL Vescovi and L De Filippis. (2010). Mild hypoxia enhances proliferation and multipotency of human neural stem cells. PLoS One 5:e8575.
26. Tsai CC, YJ Chen, TL Yew, LL Chen, JY Wang, CH Chiu and SC Hung. (2011). Hypoxia inhibits senescence and maintains mesenchymal stem cell properties through down-regulation of E2A-p21 by HIF-TWIST. Blood 117: 459–469.
27. Takubo K, G Nagamatsu, CI Kobayashi, A Nakamura-Ishizu, H Kobayashi, E Ikeda, N Goda, Y Rahimi, RS Johnson, et al. (2013). Regulation of glycolysis by pdk functions as a metabolic checkpoint for cell cycle quiescence in hematopoietic stem cells. Cell Stem Cell 12: 49–61.
28. Grayson WL, F Zhao, R Izadpanah, B Bunnell and T Ma. (2006). Effects of hypoxia on human mesenchymal stem cell expansion and plasticity in 3D constructs. J Cell Physiol 207:331–339.
29. Wang DW, B Fermor, JM Gimble, HA Awad and F Guilak. (2005). Influence of oxygen on the proliferation and metabolism of adipose derived adult stem cells. J Cell Physiol 204:184–191.
30. Moriyama M, M Osawa, SS Mak, T Ohtsuka, N Yamamoto, H Han, V Delmas, R Kageyama, F Beermann, L Larue and S Nishikawa. (2006). Notch signaling via Hes1 transcription factor maintains survival of melanoblasts and melanocyte stem cells. J Cell Biol 173:333–339.
31. Chiba S. (2006). Notch signaling in stem cell systems. Stem Cells 24:2437–2447.
32. Okura H, A Saga, Y Fumimoto, M Soeda, M Moriyama, H Moriyama, K Nagai, CM Lee, S Yamashita, et al. (2011). Transplantation of human adipose tissue-derived multilineage progenitor cells reduces serum cholesterol in hyperlipidemic Watanabe rabbits. Tissue Eng Part C Methods 17:145–154.
33. Saga A, H Okura, M Soeda, J Tani, Y Fumimoto, H Komoda, M Moriyama, H Moriyama, S Yamashita, et al. (2011). HMG-CoA reductase inhibitor augments the serum total cholesterol-lowering effect of human adipose tissue-derived multilineage progenitor cells in hyperlipidemic homozygous Watanabe rabbits. Biochem Biophys Res Commun 412:50–54.
34. Moriyama H, M Moriyama, K Sawaragi, H Okura, A Ichinose, A Matsuyama and T Hayakawa. (2013). Tightly regulated and homogeneous transgene expression in human adipose-derived mesenchymal stem cells by lentivirus with tet-off system. PLoS One 8:e66274.
35. Sekiya I, BL Larson, JR Smith, R Pochampally, JG Cui and DJ Prockop. (2002). Expansion of human adult stem cells from bone marrow stroma: conditions that maximize the yields of early progenitors and evaluate their quality. Stem Cells 20:530–541.
36. Wagner W, F Wein, A Seckinger, M Frankhauser, U Wirkner, U Krause, J Blake, C Schwager, V Eckstein, W Ansorge and AD Ho. (2005). Comparative characteristics of mesenchymal stem cells from human bone marrow, adipose tissue, and umbilical cord blood. Exp Hematol 33:1402–1416.
37. Hass R, C Kasper, S Bohm and R Jacobs. (2011). Different populations and sources of human mesenchymal stem cells (MSC): A comparison of adult and neonatal tissue-derived MSC. Cell Commun Signal 9:12.
38. Gustafsson MV, X Zheng, T Pereira, K Gradin, S Jin, J Lundkvist, JL Ruas, L Poellinger, U Lendahl and M Bondesson. (2005). Hypoxia requires notch signaling to maintain the undifferentiated cell state. Dev Cell 9:617–628.
39. Zheng X, S Linke, JM Dias, X Zheng, K Gradin, TP Wallis, BR Hamilton, M Gustafsson, JL Ruas, et al. (2008). Interaction with factor inhibiting HIF-1 defines an additional mode of cross-coupling between the Notch and hypoxia signaling pathways. Proc Natl Acad Sci U S A 105:3368–3373.
40. Pietras A, K von Stedingk, D Lindgren, S Pahlman and H Axelson. (2011). JAG2 induction in hypoxic tumor cells alters Notch signaling and enhances endothelial cell tube formation. Mol Cancer Res 9:626–636.
41. Bedogni B, JA Warneke, BJ Nickoloff, AJ Giaccia and MB Powell. (2008). Notch1 is an effector of Akt and hypoxia in melanoma development. J Clin Invest 118:3660–3670.
42. Beitner-Johnson D, RT Rust, TC Hsieh and DE Millhorn. (2001). Hypoxia activates Akt and induces phosphorylation of GSK-3 in PC12 cells. Cell Signal 13:23–27.
43. Culver C, A Sundqvist, S Mudie, A Melvin, D Xirodimas and S Rocha. (2010). Mechanism of hypoxia-induced NF-kappaB. Mol Cell Biol 30:4901–4921.
44. Rohwer N, C Dame, A Haugstetter, B Wiedenmann, K Detjen, CA Schmitt and T Cramer. (2010). Hypoxia-inducible factor 1alpha determines gastric cancer chemosensitivity via modulation of p53 and NF-kappaB. PLoS One 5:e12038.
45. Espinosa L, S Cathelin, T D'Altri, T Trimarchi, A Statnikov, J Guiu, V Rodilla, J Ingles-Esteve, J Nomdedeu, et al. (2010). The Notch/Hes1 pathway sustains NF-kappaB activation through CYLD repression in T cell leukemia. Cancer Cell 18:268–281.
46. Beverly LJ, DW Felsher and AJ Capobianco. (2005). Suppression of p53 by Notch in lymphomagenesis: implications for initiation and regression. Cancer Res 65:7159–7168.
47. Kim SB, GW Chae, J Lee, J Park, H Tak, JH Chung, TG Park, JK Ahn and CO Joe. (2007). Activated Notch1 interacts with p53 to inhibit its phosphorylation and transactivation. Cell Death Differ 14:982–991.
48. Landor SK, AP Mutvei, V Mamaeva, S Jin, M Busk, R Borra, TJ Gronroos, P Kronqvist, U Lendahl and CM Sahlgren. (2011). Hypo- and hyperactivated Notch signaling induce a glycolytic switch through distinct mechanisms. Proc Natl Acad Sci U S A 108:18814–18819.
49. Ciofani M and JC Zuniga-Pflucker. (2005). Notch promotes survival of pre-T cells at the beta-selection checkpoint by regulating cellular metabolism. Nat Immunol 6: 881–888.
50. Welford SM, B Bedogni, K Gradin, L Poellinger, M Broome Powell and AJ Giaccia. (2006). HIF1alpha delays premature senescence through the activation of MIF. Genes Dev 20:3366–3371.
51. Zhou D, J Xue, JC Lai, NJ Schork, KP White and GG Haddad. (2008). Mechanisms underlying hypoxia tolerance in Drosophila melanogaster: hairy as a metabolic switch. PLoS Genet 4:e1000221.
52. Funes JM, M Quintero, S Henderson, D Martinez, U Qureshi, C Westwood, MO Clements, D Bourboulia, RB Pedley,

S Moncada and C Boshoff. (2007). Transformation of human mesenchymal stem cells increases their dependency on oxidative phosphorylation for energy production. Proc Natl Acad Sci U S A 104:6223–6228.
53. Kawauchi K, K Araki, K Tobiume and N Tanaka. (2008). p53 regulates glucose metabolism through an IKK-NF-kappaB pathway and inhibits cell transformation. Nat Cell Biol 10:611–618.
54. Carter KL, E Cahir-McFarland and E Kieff. (2002). Epstein-barr virus-induced changes in B-lymphocyte gene expression. J Virol 76:10427–10436.
55. Ak P and AJ Levine. (2010). p53 and NF-kappaB: different strategies for responding to stress lead to a functional antagonism. FASEB J 24:3643–3652.
56. Prasad SM, M Czepiel, C Cetinkaya, K Smigielska, SC Weli, H Lysdahl, A Gabrielsen, K Petersen, N Ehlers, et al. (2009). Continuous hypoxic culturing maintains activation of Notch and allows long-term propagation of human embryonic stem cells without spontaneous differentiation. Cell Prolif 42:63–74.
57. Bash J, WX Zong, S Banga, A Rivera, DW Ballard, Y Ron and C Gelinas. (1999). Rel/NF-kappaB can trigger the Notch signaling pathway by inducing the expression of Jagged1, a ligand for Notch receptors. EMBO J 18:2803–2811.

Address correspondence to:
Dr. Hiroyuki Moriyama
Pharmaceutical Research and Technology Institute
Kinki University
3-4-1 Kowakae
Higashi-Osaka
Osaka 577-8502
Japan

E-mail: moriyama@phar.kindai.ac.jp

Received for publication December 26, 2013
Accepted after revision May 15, 2014
Prepublished on Liebert Instant Online May 30, 2014

Knee Surg Sports Traumatol Arthrosc
DOI 10.1007/s00167-014-3142-y

KNEE

Anterior knee symptoms after double-bundle ACL reconstruction with hamstring tendon autografts: an ultrasonographic and power Doppler investigation

Takashi Kanamoto · Yoshinari Tanaka · Yasukazu Yonetani · Keisuke Kita · Hiroshi Amano · Masashi Kusano · Shinji Hirabayashi · Shuji Horibe

Received: 19 August 2013 / Accepted: 12 June 2014

Abstract
Purpose Anterior knee pain related to the donor site is a frequent complication of anterior cruciate ligament reconstruction (ACLR) with bone-patellar tendon-bone autograft tissue. Even when hamstring tendon (HT) grafts are used instead, symptoms such as mild pain and discomfort can still occur. The purpose of this study was to elucidate the pathophysiology of anterior knee symptoms after ACLR with HT autografts.
Methods Fifty-seven patients (22 men and 35 women; mean age, 24.7 years) who underwent anatomic double-bundle ACLR with HT autografts were examined 6 months post-operatively. The presence of anterior knee symptoms, anterior knee laxity, range of motion, and muscle strength were assessed. Changes in patellar tendon and infrapatellar fat pad (IFP) morphology and blood flow were also evaluated using ultrasound. Potential variables affecting the presence of anterior knee symptoms were subjected to univariate analysis and multivariate logistic regression analysis to identify independent risk factors.
Results Six months post-operatively, the total incidence of anterior knee symptoms was 56.1 % (32/57). According to univariate analysis, age, quadriceps strength, and increased blood flow in the IFP were significantly associated with the presence of anterior knee symptoms. Multivariate logistic regression analysis revealed that increased blood flow in the IFP was an independent factor for the presence of anterior knee symptoms (odds ratio 5.0; 95 % confidence interval 1.3–19.9). There were no significant findings inside the patellar tendon.
Conclusions Increased blood flow in the IFP was identified as an independent factor for the presence of anterior knee symptoms 6 months after ACLR with HT autografts. The ultrasound evaluation can help to define precisely the origin of anterior knee symptoms after ACLR with HT autografts.
Level of evidence Case series with no comparison groups, Level IV.

Keywords Anterior knee problems/symptoms · ACL reconstruction · Ultrasound · Infrapatellar fat pad · Increased blood flow

T. Kanamoto (✉) · S. Hirabayashi
Department of Rehabilitation, Osaka Rosai Hospital, 1179-3, Nagasone-cho, Kita-ku, Sakai, Osaka 597-8025, Japan
e-mail: takanamoto2@gmail.com

Y. Tanaka · K. Kita · H. Amano
Department of Orthopaedic Surgery, Osaka Rosai Hospital, Sakai, Japan

Y. Yonetani
Department of Orthopaedic Surgery, Osaka University Graduate School of Medicine, Osaka University, Osaka, Japan

M. Kusano
Department of Orthopaedic Surgery, Kansai Rosai Hospital, Sakai, Japan

S. Horibe
Faculty of Comprehensive Rehabilitation, Osaka Prefecture University, Habikino, Osaka, Japan

Introduction

Anterior knee pain, generally related to the donor site, is one of the most frequent complications after anterior cruciate ligament reconstruction (ACLR) with bone-patellar tendon-bone (BTB) autografts and has the potential to impede rehabilitation and a return to sports activities [12, 16, 26]. Even when hamstring tendon (HT) grafts are used for ACLR instead, anterior knee symptoms such as mild pain and discomfort during daily activities and sports can

Published online: 01 July 2014

occur at an incidence of 9.3–32.2 % [14, 16, 17, 20]. Several factors have been found to contribute to anterior knee symptoms after ACLR with HT grafts, such as knee extension deficits [12, 21], low quadriceps muscle power [17], and residual anterior instability [26]; the pathophysiology, however, is still unknown.

Anterior knee symptoms during activities of daily living and sports can also be caused by disorders of the knee extensor mechanism and surrounding soft tissues, such as patellar tendinopathy and Hoffa's disease [5, 18]. Because surgical treatment has the possibility to affect anterior knee structures [24], the anterior knee symptoms after ACLR could be derived from the abnormal property of the structures such as patellar tendon (PT) and infrapatellar fat pad (IFP). Anterior knee structures are closely related and must be seen as a single mechanism, often making it difficult to distinguish focal lesions [23]. Ultrasound has been established as an effective imaging technique for evaluation of the knee extensor mechanism and surrounding soft tissues, although it is not advantageous when it comes to detection of cartilage lesions of the knee [2]. Studies on patellar tendinopathy have shown an association between clinical symptoms such as pain and morphologic and blood flow changes in the tendon [5, 10]. For the present study, ultrasound imaging was used to evaluate anterior knee structures and elucidate the pathophysiology of anterior knee symptoms after ACLR with HT autografts.

The purpose of this study was to determine the risk factors for anterior knee symptoms after ACLR with HT autografts. Demographic data and clinical results such as anterior knee laxity, knee range of motion, and thigh muscle strength were examined, and ultrasound evaluations of the morphology and vascularity of the patellar tendon and infrapatellar fat pad were performed. The hypothesis was that changes in morphology and vascularity of anterior knee structures would be associated with the incidence of anterior knee symptoms after ACLR with HT autografts.

Materials and methods

Between April 2010 and March 2012, primary anatomic double-bundle ACL reconstruction with HT autografts was performed on 323 knees. Of those, 57 patients provided informed consent to evaluate 57 knees by ultrasound 6 months post-operatively. As ultrasound examination was performed only 1 day a week, patients represented 17 % of the available cohort, with no selection bias present.

Surgical procedure and post-operative rehabilitation

Anatomic double-bundle ACL reconstruction with HT grafts was performed based on age and activity level as previously described [25]. Post-operatively, all patients underwent the same rehabilitation protocol. Briefly, the knee was immobilized with a brace for 2 weeks, partial weight bearing was allowed at 3 weeks, and full weight bearing was permitted at 4 weeks. Jogging and running were allowed for 3–4 months, followed by a return to previous sports activities at 6–9 months.

Assessment of anterior knee symptoms

Patients answered a 13-item self-report questionnaire, known as the Anterior Knee Pain Scale (also known as the Kujala scale [13]), to examine the incidence of symptoms during six activities (walking, running, jumping, climbing stairs, squatting, and sitting for prolonged periods with the knee bent) considered to be specifically associated with anterior knee pain syndrome [13, 22]. We dichotomized answers into either 'no difficulty' or 'other' categories; patients who selected 'other' categories were considered to have anterior knee symptoms.

Subjective evaluation and physical examination

At 6 months after ACLR, subjective evaluation was performed using the IKDC subjective knee form and physical examinations including anterior knee laxity as measured by the KT-2000 arthrometer (MEDmetric, San Diego, CA), heel-height difference (HHD), and isokinetic thigh muscle strength measured by the Cybex 6000 isokinetic dynamometer (Lumex, Inc., Ronkonkoma, NY) were performed. Parameters used were the average side-to-side differences in anterior laxity at manual maximum force and the ratio of peak extensor and flexor torques at 60°/s between involved and uninvolved limbs.

Ultrasound evaluation

Ultrasonography was performed using a Prosound II SSD-6500SV linear, multi-frequency (5–13 MHz) array transducer (ALOKA, Tokyo, Japan). The PT and IFP were completely scanned along longitudinal and transverse planes. With grayscale ultrasound, morphologic tendon changes (thickening of hypoechoic areas) were registered on a standard form [10]. Power Doppler was used to diagnose blood flow in the PT and IFP [5, 7]. To maximize sensitivity to any flow, the lowest pulse repetition frequency and wall filter were applied. When more blood flow signal was detected compared to contralateral knees, it was recorded as increased blood flow (Fig. 1). Two examiners examined five randomly selected subjects with regard to intra- and inter-reproducibility of ultrasound

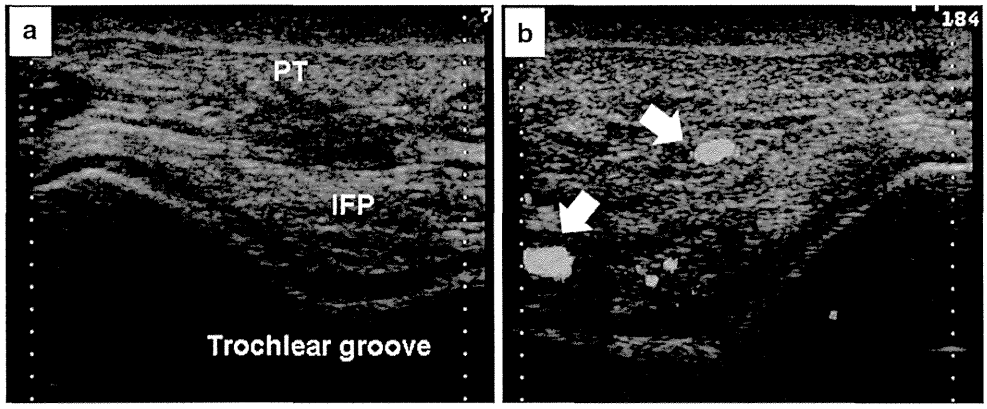

Fig. 1 Representative ultrasound image of knee. The transverse planes of both knees of a 51-year-old female patient with post-operative anterior knee symptoms during squatting, running, and climbing stairs. Articular cartilage in the trochlear groove was seen in the viewing field, and the infrapatellar fat pad (IFP) was observed between the patellar tendon (PT) and femoral trochlear groove. **a** Non-operated right knee. No blood flow signal was observed in the IFP. **b** Operated left knee. Increased blood flow signal was observed in the IFP (*arrows*)

examination, for which a perfect agreement was observed. All examinations in this study were completed by an orthopaedic surgeon who was experienced in musculoskeletal ultrasound and blinded to clinical outcome assessments.

Ethical standards

Our study protocol abided by standards set by the Helsinki Declaration, and all experiments in this study were conducted in accordance with a protocol approved by the Ethical Committee of Osaka Rosai Hospital.

Statistical analysis

Continuous variables are expressed as mean ± SD. The χ^2 test and Fisher's exact test were used to compare categorical variables between patients with and without anterior knee symptoms. Unpaired Student's t test or Mann–Whitney U test were performed for univariate analysis of continuous variables between groups. After determining variables associated with anterior knee symptoms according to univariate analysis, multivariate logistic regression analysis was performed. All analyses were performed using SPSS (SPSS Inc., Chicago, IL), with $P < 0.05$ considered statistically significant.

Sample size calculation indicated that a total of 34 patients would be required to show significant changes in a chi-square test with an α level of 0.05 and a β level of 80 %. For comparison of isokinetic thigh muscle strength between the group with anterior knee pain and the group without anterior knee pain, a total of 52 patients was required to show a significant difference at an α level of 0.05 and a β level of 80 %.

Results

Patient characteristics and incidences of anterior knee symptoms

Participant characteristics are summarized in Table 1. Thirty-two patients (56.1 %) showed symptoms during at least one of six activities, but none had severe symptoms that disrupted activities of daily living. According to univariate analysis, age was significantly associated with anterior knee symptoms ($P = 0.012$). Gender, worker-to-student ratio, pre-injury Tegner activity level, pre-operative quadriceps torque at 60°/s, meniscal lesions, and articular cartilage defects did not correlate with the presence of anterior knee symptoms (Fig. 2).

Subjective evaluation and physical examination at post-operative follow-up

Average IKDC subjective scores 6 months after ACLR were 54.7 ± 6.0 and 56.4 ± 5.2 for the groups with and without anterior knee symptoms, respectively (n.s.). No significant difference was observed in anterior knee laxity or in HDD between the groups with and without anterior knee symptoms. Isokinetic testing showed that quadriceps torque was restored less effectively in the group with anterior knee symptoms (64.0 ± 18.3 %) than the group without symptoms (82.9 ± 15.4 %) ($P = 0.0004$) (Table 2).

Ultrasound findings

Ultrasound results did not reveal abnormal changes in morphology such as hypoechoic lesions and blood flow in

Table 1 Patient demographics

Variable	All	Men	Women	Significance[§] (*P* value)
No. cases/no. knees	57	22	35	
Age (range) in years	24.7 (13–51)	27.0 (15–45)	23.3 (13–51)	NS
Worker/student	20/37	8/14	12/23	NS
Median pre-injury Tegner activity level (range)	7 (4–9)	7 (4–9)	9 (4–9)	$P = 0.01$[†]
Pre-operative quadriceps torque 60°/s	61.3 ± 17.2	61.1 ± 20.4	61.5 ± 14.9	NS
Treatment for meniscal lesion (no. cases of partial resection/repair)	31	15	16	NS
Articular cartilage defect (outerbridge classification ≥II)	18	8	10	NS

[§] Statistically significant difference between men and women

[†] Mann–Whitney *U* test

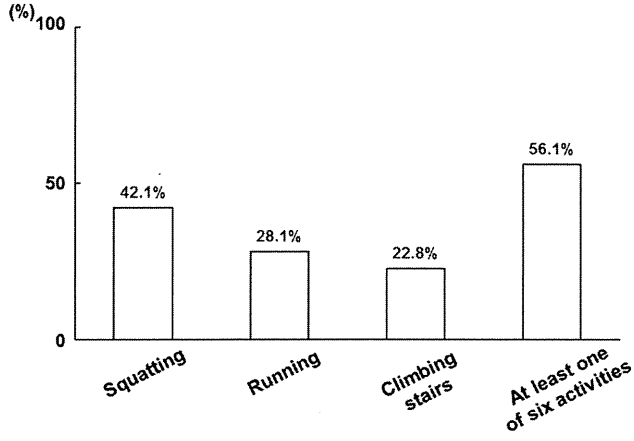

Fig. 2 Incidence of anterior knee symptoms during activities of daily living. Six months post-operatively, anterior knee symptoms were reported in 24 patients (42.1 %) when squatting, 16 (28.1 %) when running, and 13 (22.8 %) when climbing stairs. Thirty-two patients (56.1 %) showed symptoms during at least one of six activities (walking, running, jumping, climbing stairs, squatting, and sitting for prolonged periods with the knee bent)

Table 2 Comparison of physical examinations among those with and without AKP

Variable	Group with anterior knee pain	Group without anterior knee pain	Significance (*P* value)
No. cases	32	25	
Anterior knee laxity[§]			
Mean (range) in mm	0.7 ± 0.8	0.5 ± 1.2	NS
≤2 mm (%)	95 8	91.7	NS
Knee flexion contracture			
HHD ≥1.0 cm (%)	34.4	12.5	NS
Quadriceps torque at 60°/s[†]	68.4 ± 14.8	85.4 ± 15.1	$P = 0.0004$
Hamstrings torque at 60°/s[†]	82.1 ± 15.4	87.2 ± 12.5	NS

NS not significant *HHD* heel-height difference

[§] The side-to-side difference with the KT-2000 arthrometer at maximum manual force

[†] Values are expressed as a percentage of the uninvolved side

the PT. With the IFP, however, 28 patients (87.5 %) in the group with anterior knee symptoms and 13 (52.0 %) in the group without symptoms showed increased blood flow (Table 3). The relationship between the presence of anterior knee symptoms and increased blood flow in the IFP was significant ($P = 0.003$).

Multivariate logistic regression analysis

According to univariate analysis, age, quadriceps torque, and increased blood flow in the IFP were included as factors of anterior knee symptoms. Patients were grouped by whether they were either 18 years old and younger or older than 18, given the consideration of biological growth, and 80 % of the uninvolved limbs were used as a cut-off point to indicate quadriceps torque. Multivariate logistic regression analysis revealed that quadriceps torque (odds ratio 3.5; 95 % confidence interval 1.0–11.7) and increased blood flow in the IFP (odds ratio 5.0; 95 % confidence interval 1.3–19.9) were independent factors associated with the presence of anterior knee symptoms (Table 3).

Discussion

The most important finding of the present study was that increased blood flow in the IFP was identified as an independent factor associated with the presence of anterior

Table 3 Multivariate logistic regression analysis of risk factors for anterior knee symptoms

Variables	No. cases	Patients with anterior knee symptoms	Odds ratio	95 % confidence interval	Significance (*P* value)
Age (years)					
≤18	27	12 (44.4 %)	1.0		
18<	30	20 (67.7 %)	1.7	0.5–5.7	0.4
Quadriceps torque at 60°/s					
80 %≤	25	9 (36.0 %)	1.0		
<80 %	32	23 (71.9 %)	3.5	1.0–11.7	0.04
Increased blood flow in the infrapatellar fat pad					
No	16	4 (25.0 %)	1.0		
Yes	41	28 (68.3 %)	5.0	1.3–19.9	0.02

knee symptoms 6 months after ACLR with HT autografts, although there were no abnormal changes in the PT.

In this study, the incidence of anterior knee symptoms was 56.1 %. In previous reports, incidences of anterior knee symptoms after ACLR with HT grafts were 12.5–32.2 % [14]. A possible explanation for this discrepancy is different assessment methods. With no agreement on exact diagnostic criteria, investigators have diagnosed anterior knee symptoms with their own methods [16, 26] or systems such as the IKDC score [1], patellofemoral pain score [9] or Kujala patellofemoral score (the Anterior Knee Pain Scale) [11]. Among these, we selected the Anterior Knee Pain Scale and examined the incidence of anterior knee symptoms during these six activities considered to be associated specifically with anterior knee pain syndrome [22]. We removed symptom severity from our consideration, given that none of our patients experienced pain during these activities. We also assessed symptoms at 6 months post-operatively, while most other studies were performed at least 2 years after ACLR [14]. Niki et al. [17] recently reported that the prevalence of anterior knee pain was 42.0 % 3 months post-operatively, falling to 11.1 % after 2 years. These issues make it difficult to compare our incidence of anterior knee symptoms with other reported rates.

There appears to be consensus in the literature that regaining thigh muscle strength after any type of autograft is essential for avoiding future anterior knee problems [12, 19]. Muneta et al. [15] reported that patients' subjective evaluations of their ACL reconstruction with HT or BTB autografts were worse if quadriceps or hamstring strength was less than that of the contralateral side. Niki et al. [17] reported that quadriceps peak torque at 60°/s, not donor site morbidity, was associated with anterior knee pain development 2 years post-operatively. Although it remains unclear whether reduced quadriceps torque was a cause or consequence of anterior knee pain and what the underlying mechanisms are [16, 17], there is no doubt about the importance of thigh muscle strength in patients after ACLR.

The IFP is an intracapsular, extrasynovial adipose tissue that fills the anterior knee compartment and is richly vascularized and innervated [8], but its precise function is unknown [3, 24]. Although the pathophysiology is not yet confirmed, several studies have described chronic hyperplasia of the IFP as a possible cause of anterior knee symptoms [18, 24]. More recent articles, on the other hand, highlighted the IFP as a biochemical modulator of inflammatory and destructive responses in the injured knee [6, 28]. In human osteoarthritic joints and animal models, nociceptive nerve fibres present in the IFP or infiltrating immune cells can cause anterior knee symptoms [4]. In the present study, ultrasonography showed increased blood flow in the IFP more frequently in patients with anterior knee symptoms than in those without symptoms. Abnormal blood flow can be observed in several clinical situations [27, 28]. Some studies have shown that intratendinous flow is associated with symptomatic patellar and Achilles tendinopathy, which supports monitoring tendon neovascularization as a diagnostic indicator of critical situations [5]. To our knowledge, this study is the first to utilize ultrasound evaluation of blood flow in the IFP, although the exact mechanism underlying the increased blood flow requires further investigation.

The present study has some limitations. First, it was a cross-sectional study based on a relatively small sample size, but still revealed new information about the pathophysiology of anterior knee symptoms after ACLR with HT autografts and tested ultrasound as a possible evaluation tool. Second, the short-term follow-up might not be related to long-term clinical outcomes such as anterior knee symptoms. Investigation at a relatively early stage can be meaningful, however, because it is preferable to minimize subjective symptoms early before they impede rehabilitation and patients return to sports activities [16]. Finally, no patients experienced highly severe anterior knee symptoms in this study. As such, we were unable to examine the relationship between the blood flow in the IFP and severity of anterior knee symptoms.

The clinical relevance of this study is that the ultrasound evaluation can be helpful when defining the precise origin of anterior knee symptoms after ACLR with HT autografts.

Conclusion

Quadriceps torque and increased blood flow in the IFP were identified as independent factors associated with the presence of anterior knee symptoms 6 months after ACLR with HT autografts, although there were no abnormal changes inside the PT. Age, gender, intra-articular lesions, and knee extension deficit were not independent variables that affected the presence of anterior knee symptoms.

References

1. Aglietti P, Buzzi R, Zaccherotti G, De Biase P (1994) Patellar tendon versus doubled semitendinosus and gracilis tendons for anterior cruciate ligament reconstruction. Am J Sports Med 22:211–217
2. Bayar A, Turhan E, Ozer T, Keser S, Ege A, Erdem Z (2008) The fate of patellar tendon and infrapatellar fat pad after arthroscopy via central portal. Knee Surg Sports Traumatol Arthrosc 16: 1114–1120
3. Bohnsack M, Wilharm A, Hurschler C, Ruhmann O, Stukenborg-Colsman C, Wirth CJ (2004) Biomechanical and kinematic influences of a total infrapatellar fat pad resection on the knee. Am J Sports Med 32:1873–1880
4. Clockaerts S, Bastiaansen-Jenniskens YM, Runhaar J, Van Osch GJ, Van Offel JF, Verhaar JA, De Clerck LS, Somville J (2010) The infrapatellar fat pad should be considered as an active osteoarthritic joint tissue: a narrative review. Osteoarthritis Cartilage 18:876–882
5. Cook JL, Ptazsnik R, Kiss ZS, Malliaras P, Morris ME, De Luca J (2005) High reproducibility of patellar tendon vascularity assessed by colour Doppler ultrasonography: a reliable measurement tool for quantifying tendon pathology. Br J Sports Med 39:700–703
6. Distel E, Cadoudal T, Durant S, Poignard A, Chevalier X, Benelli C (2009) The infrapatellar fat pad in knee osteoarthritis: an important source of interleukin-6 and its soluble receptor. Arthritis Rheum 60:3374–3377
7. Dragoo JL, Samimi B, Zhu M, Hame SL, Thomas BJ, Lieberman JR, Hedrick MH, Benhaim P (2003) Tissue-engineered cartilage and bone using stem cells from human infrapatellar fat pads. J Bone Joint Surg Br 85:740–747
8. Dragoo JL, Johnson C, McConnell J (2012) Evaluation and treatment of disorders of the infrapatellar fat pad. Sports Med 42:51–67
9. Eriksson K, Anderberg P, Hamberg P, Lofgren AC, Bredenberg M, Westman I, Wredmark T (2001) A comparison of quadruple semitendinosus and patellar tendon grafts in reconstruction of the anterior cruciate ligament. J Bone Joint Surg Br 83:348–354
10. Hoksrud A, Ohberg L, Alfredson H, Bahr R (2008) Color Doppler ultrasound findings in patellar tendinopathy (jumper's knee). Am J Sports Med 36:1813–1820
11. Ibrahim SA, Al-Kussary IM, Al-Misfer AR, Al-Mutairi HQ, Ghafar SA, El Noor TA (2005) Clinical evaluation of arthroscopically assisted anterior cruciate ligament reconstruction: patellar tendon versus gracilis and semitendinosus autograft. Arthroscopy 21:412–417
12. Kartus J, Movin T, Karlsson J (2001) Donor-site morbidity and anterior knee problems after anterior cruciate ligament reconstruction using autografts. Arthroscopy 17:971–980
13. Kujala UM, Jaakkola LH, Koskinen SK, Taimela S, Hurme M, Nelimarkka O (1993) Scoring of patellofemoral disorders. Arthroscopy 9:159–163
14. Mohtadi NG, Chan DS, Dainty KN, Whelan DB (2011) Patellar tendon versus hamstring tendon autograft for anterior cruciate ligament rupture in adults. Cochrane Database Syst Rev 9: CD005960
15. Muneta T, Sekiya I, Ogiuchi T, Yagishita K, Yamamoto H, Shinomiya K (1998) Objective factors affecting overall subjective evaluation of recovery after anterior cruciate ligament reconstruction. Scand J Med Sci Sports 8:283–289
16. Niki Y, Matsumoto H, Hakozaki A, Kanagawa H, Toyama Y, Suda Y (2011) Anatomic double-bundle anterior cruciate ligament reconstruction using bone-patellar tendon-bone and gracilis tendon graft: a comparative study with 2-year follow-up results of semitendinosus tendon grafts alone or semitendinosus-gracilis tendon grafts. Arthroscopy 27:1242–1251
17. Niki Y, Hakozaki A, Iwamoto W, Kanagawa H, Matsumoto H, Toyama Y, Suda Y (2012) Factors affecting anterior knee pain following anatomic double-bundle anterior cruciate ligament reconstruction. Knee Surg Sports Traumatol Arthrosc 20:1543–1549
18. Ogilvie-Harris DJ, Giddens J (1994) Hoffa's disease: arthroscopic resection of the infrapatellar fat pad. Arthroscopy 10:184–187
19. Risberg MA, Holm I, Tjomsland O, Ljunggren E, Ekeland A (1999) Prospective study of changes in impairments and disabilities after anterior cruciate ligament reconstruction. J Orthop Sports Phys Ther 29:400–412
20. Sandon A, Werner S, Forssblad M (2014) Factors associated with returning to football after anterior cruciate ligament reconstruction. Knee Surg Sports Traumatol Arthrosc. [Epub ahead of print]
21. Shelbourne KD, Trumper RV (1997) Preventing anterior knee pain after anterior cruciate ligament reconstruction. Am J Sports Med 25:41–47
22. Singer B, Singer K (2009) Anterior knee pain scale. Aust J Physiother 55:140
23. Skiadas V, Perdikakis E, Plotas A, Lahanis S (2013) MR imaging of anterior knee pain: a pictorial essay. Knee Surg Sports Traumatol Arthrosc 21:294–304
24. Sonnery-Cottet B, Archbold P, Zayni R, Thaunat M, Bortolletto J, Fayard JM, Chambat P (2011) High lateral portal for sparing the infrapatellar fat-pad during ACL reconstruction. Orthop Traumatol Surg Res 97:870–873
25. Tanaka Y, Yonetani Y, Shiozaki Y, Kanamoto T, Kita K, Amano H, Kusano M, Hirakawa M, Horibe S (2013) MRI analysis of single-, double-, and triple-bundle anterior cruciate ligament grafts. Knee Surg Sports Traumatol Arthrosc 22(7):1541–8
26. Tsuda E, Okamura Y, Ishibashi Y, Otsuka H, Toh S (2001) Techniques for reducing anterior knee symptoms after anterior cruciate ligament reconstruction using a bone-patellar tendon-bone autograft. Am J Sports Med 29:450–456
27. Vedung T, Werner M, Ljung BO, Jorfeldt L, Henriksson J (2011) Blood flow to the extensor carpi radialis brevis muscle following adrenaline infusion in patients with lateral epicondylitis. J Hand Surg Am 36:1974–1980
28. Witonski D, Wagrowska-Danilewicz M, Raczynska-Witonska G (2005) Distribution of substance P nerve fibers in osteoarthritis knee joint. Pol J Pathol 56:203–206

J Orthopaed Traumatol
DOI 10.1007/s10195-014-0301-3

BRIEF COMMUNICATION

Patellar mobility can be reproducibly measured using ultrasound

Takashi Kanamoto · Yoshinari Tanaka · Yasukazu Yonetani · Keisuke Kita · Hiroshi Amano · Masashi Kusano · Mie Fukamatsu · Shinji Hirabayashi · Shuji Horibe

Received: 14 November 2013 / Accepted: 12 May 2014

Abstract The present study was performed to examine the reliability of ultrasound in evaluating patellar mobility in the superior–inferior direction. Twelve healthy men volunteered for the study. Patellar mobility in the superior–inferior direction during isometric knee extension contraction with the knee immobilized in a semi-flexed knee brace was measured using ultrasound. Both intra-observer and inter-observer reliability were assessed by intra-class correlation coefficients (ICCs). Bland–Altman analysis was used for assessing agreement between measurements. ICC values were excellent for both intra-observer and inter-observer reliability at 0.97 and 0.93, respectively. In 95 % of measurements, the same observer measured within −0.55 to 0.61 mm, while different observers measured within −0.82 to 0.85 mm. In conclusion, patellar mobility in the superior–inferior direction during an isometric knee extension exercise can be reproducibly measured using ultrasound.
The level of evidence VI (basic study of a novel evaluation method).

T. Kanamoto (✉) · S. Hirabayashi
Department of Rehabilitation, Osaka Rosai Hospital,
1179-3 Nagasone-cho, Kita-ku, Sakai, Osaka 597-8025, Japan
e-mail: takanamoto2@gmail.com

Y. Tanaka · Y. Yonetani · K. Kita · H. Amano · M. Kusano · S. Horibe
Department of Orthopaedic Surgery, Osaka Rosai Hospital,
1179-3 Nagasone-cho, Kita-ku, Sakai, Osaka 597-8025, Japan

M. Fukamatsu
Department of Clinical Laboratory, Osaka Rosai Hospital,
1179-3 Nagasone-cho, Kita-ku, Sakai, Osaka 597-8025, Japan

Published online: 04 June 2014

Keywords Patellar mobility · Ultrasound · Rehabilitation · Isometric knee extension exercise · Reliability

Introduction

To prevent postoperative complications, it is important to regain normal patellar mobility after knee surgeries such as anterior cruciate ligament reconstruction and total knee arthroplasty. Patellar immobility leads to decreased range of motion, quadriceps inhibition, altered gait pattern, and prolonged rehabilitation [1]. Thus, multidirectional mobilization of the patella and quadriceps muscle setting exercises are initiated in the early postoperative period to improve patellar mobility and quadriceps function. Despite the importance of this being generally accepted, a single gold standard evaluation method of patellar mobility has not been established [2–4].

With the recent development of high-resolution probes, the use of musculoskeletal ultrasound has significantly increased [5]. The superficial localization of the knee extensor apparatus, including the patella and patellar tendon, makes it suitable for ultrasound evaluation [6, 7]. The purpose of this report was to determine if ultrasonography can be useful in evaluating patellar mobility in the superior–inferior direction during an isometric knee extension exercise.

Materials and methods

Participants

Twelve healthy men with no signs of musculoskeletal injury or disorder that would prevent their participation